UNIVERSITY OF CALIFORNIA SAN DIEGO

Dendrite and axon morphology as distinguishing properties of excitatory and inhibitory neuronal cell types in the *Xenopus laevis* optic tectum

A thesis submitted in partial satisfaction of the requirements for the degree

Master of Science

in

Biology

by

Vi Phuong Dang

Committee in charge:

Professor Hollis Cline, Chair
Professor Yishi Jin, Co-Chair
Professor Nicholas Spitzer

2019

The Thesis of Vi Phuong Dang is approved, and it is acceptable in quality and form for publication on microfilm and electronically:

_____

_____
Co-Chair

_____
Chair

University of California San Diego

2019

TABLE OF CONTENTS

LIST OF FIGURES

LIST OF TABLES

ACKNOWLEDGMENTS

I would like to thank Dr. Hollis Cline for her support as my advisor and committee chair. I have learned so much from being in her lab and hearing all of her feedback and ideas. I am also grateful for her guidance and advice for both my thesis and this project.

I would like to thank Dr. Yishi Jin and Dr. Nicholas Spitzer for their time and support as the members of my committee.

Sections 2.3 and 3.3 are co-authored with Dang, Vi P. and Faulkner, Regina L. The thesis author was the primary author of these sections.

I must also thank Dr. Regina Faulkner for being a patient, understanding, and inspirational mentor and collaborator for this project, which could not have been done without her. She taught me everything I know and contributed to many essential parts of this project.

I would also like to thank all members of the Cline lab for their guidance and support throughout my time in the lab.

Lastly, I would like to thank NIH for their support by funding this project.

ABSTRACT OF THE THESIS

Dendrite and axon morphology as distinguishing properties of excitatory and inhibitory neuronal cell types in the *Xenopus laevis* optic tectum

by

Vi Phuong Dang

Master of Science in Biology

University of California San Diego, 2019

Professor Hollis T. Cline, Chair
Professor Yishi Jin, Co-Chair

The brain contains a diverse array of neurons that vary in complexity. Investigating the properties and connectivity of these neurons is essential to identifying the relationships between brain function, behavior, and disease. A useful animal model for studying the brain is the albino *Xenopus laevis* tadpole due to its transparent skin and visible external development. One region of interest is the optic tectum, a midbrain region homologous to the mammalian superior colliculus, that is responsible for visual processing and visuomotor behaviors. While the optic tectum is known to be responsible for mediating visually-guided behaviors, knowledge is limited

on what neuronal cell types exist in the optic tectum and how these neurons interact to cause behavior. In order to characterize excitatory and inhibitory neuronal cell types in the optic tectum, we used live imaging of single cells expressing GFP in Stage 47 albino *Xenopus laevis* and reconstructed the neurons' dendritic and axonal morphology. Post hoc GABA immunolabeling of cross sections was used to characterize the cell as inhibitory or excitatory. Here we present the comparison of excitatory and inhibitory neurons in the optic tectum based on their dendritic and axonal characteristics. Specifically, we compared their total axon and dendrite length, axon and dendrite branch tip number, number of primary dendrites, deepest dendrite depth, and axon projections, to investigate whether any of these parameters may differentiate between excitatory and inhibitory neuronal cell types. We also experimented to optimize the published SWITCH protocol for our methods to improve our post hoc GABA immunostaining.

INTRODUCTION

Behavior is dictated by the multifaceted cellular interactions within neural circuits in response to different sensory and environmental stimuli. Thus, to understand how a behavioral response is formed, or in other words, why something behaves a certain way, we must first understand the brain regions and circuits involved in facilitating such behaviors. To begin unraveling the complexities of neural circuits, it is crucial to identify and characterize the most basic components of a circuit, which are the cells that comprise it.

One particular circuit of interest is the retinotectal circuit that is central to the visual system in amphibians, and develops in response to visual input (Aizenman and Cline, 2007). This neural circuit involves communication between retinal ganglion cells (RGC) and neurons in the optic tectum (Liu et al., 2016). The optic tectum is a midbrain region homologous to the mammalian superior colliculus, and is a hub for visual information processing to regulate sensorimotor (Felsen and Mainen, 2012) and survival behaviors, such as prey capture and predator avoidance (King, 2004). Although it is understood that the optic tectum is important for controlling these behaviors, it is still unclear as to how exactly these behavioral responses are formulated by the retinotectal circuit as several different models have been proposed (Bianco and Engert, 2015; Felch et al., 2016).

A useful animal model for studying the retinotectal circuit in the optic tectum is the albino *Xenopus laevis* tadpole. These animals are externally developing and their skin is transparent during early stages of development, making their brains more accessible for *in vivo* experimentation and analyses (Cline, 2001). Aside from these practical reasons, the developing *Xenopus* tadpole also serves as an interesting animal model because their visual experiences are instrumental in guiding the development of the retinotectal circuit (Pratt et al., 2016), especially at stages 44-47 (Nieuwkoop and Faber, 1956) of development (Liu et al., 2016). At stage 47 in

developing *Xenopus* tadpoles, the retinotectal circuit supports and directs behavioral responses to visual stimuli and experiences (Miraucourt et al., 2012). This makes studying stage 47 of developing *Xenopus* tadpoles pertinent to understanding the relationship between the retinotectal circuitry and behavior. Despite this, tectal neurons have only been classified by their morphology and neurotransmitter expression in adult frogs (Rybickka and Udin, 1994; Li and Fite, 1998), but not comprehensively in stage 47 *Xenopus* tadpoles (Miraucourt et al., 2012; Lázár, 1973). We will use a combination of *in vivo* imaging, whole mount imaging of fixed brains, and posthoc immunohistochemistry to characterize the morphological features of excitatory and inhibitory neurons in the stage 47 optic tectum.

1.1 SWITCH Protocol Optimization for the *Xenopus laevis* Model

Understanding cellular anatomy, molecular interactions, and neurotransmission is essential to identifying the intricacies of complex circuits and behaviors controlled by the brain. One approach to studying these neural networks is the application of immunohistochemistry (IHC), which can be used to analyze the distribution of antigens and cell markers.

Neurotransmitter expression is a fundamental characterization of neurons as it produces the excitation and inhibition signals necessary to facilitate cellular communication within a neural circuit. In the developing *Xenopus* optic tectum, GABA is the main inhibitory neurotransmitter (Miraucourt et al., 2012). GABAergic neurotransmission is key for maintaining the balance of excitation and inhibition (Akerman, 2006), and refining receptive visual fields of optic tectal neurons across several developmental stages (Tao and Poo, 2005). In stage 47 *Xenopus*, GABA is hyperpolarizing (Akerman and Cline, 2007) and GABA immunoreactivity is more uniform in the optic tectum (Miraucourt et al., 2012). Tectal neurons that are not GABAergic are distinctly excitatory (Miraucourt et al., 2012). Classifying these GABAergic

(hereinafter inhibitory) and non-GABAergic (hereinafter excitatory) tectal neurons may be vital to understanding how different neuronal cell types underlie different behavioral responses.

Although IHC has allowed for many advances in scientific research, its usage is limited to thinly sectioned tissue due to poor antibody penetration of thick tissue blocks or whole mount samples (Murray et al., 2015). This is the case in the *Xenopus* optic tectum, where GABA IHC works efficiently with sectioned samples (Figure 5G), but fails in whole mount brain tissue (Figure 1). Though tissue sectioning allows for efficient IHC, it severs connections within the brain and makes it difficult to visualize whole neurons and neural circuits. When performing IHC in whole mount samples, there is highly saturated fluorescence and antibody binding at the top and bottom surfaces of the tissue sample, but poor binding and signal in the middle regions (Murray et al., 2015). Other problems with tissue sectioning for IHC include losing sections or uneven sectioning due to faulty equipment. This has fueled multiple efforts to formulate alternative methods for multiplexed visualization of intact biological systems. Some of these novel visualization techniques include expansion microscopy (Freifeld et al., 2017), CLARITY (Chung et al., 2013), and SWITCH (Murray et al., 2015).

Two of the novel methods, expansion microscopy (ExM) and CLARITY, operate through very similar approaches to achieve the goal of improving the visualization of intact neural systems. The ExM method was able to improve the resolution and labeling of fine cellular processes in the intact zebrafish optic tectum (Freifeld et al., 2017), while CLARITY was able to make an adult mouse brain transparent to allow for more efficient antibody penetration and high resolution imaging. The ExM technique relies on the embedment of the tissue sample in a polyelectrolyte gel before submersion in water to swell the sample and resolve the intact molecular networks. Similarly, CLARITY involves the infusion and hybridization of hydrogel monomers with the tissue sample before electrophoretic tissue clearing is done to remove

endogenous lipids (Chung et al., 2013). In contrast, the SWITCH approach is much simpler as it does not require any special mounting of the sample or creating a hybrid structure with gel components, which could be more difficult with a sample as small and fragile as the *Xenopus* tadpole brain.

The SWITCH protocol works to improve antibody penetration and uniform immunolabeling through combinations of various buffers that either suppress or facilitate chemical reactions in a tissue sample (Murray et al., 2015). These specifically controlled reactions enable uniform antibody penetration by preventing antibody binding until the antibody has equilibrated throughout the depth of the tissue (Murray et al., 2015). The antibody binding process is then "switched on" by changing the reagent of incubation (Murray et al., 2015). It was shown in Murray et al., 2015 that the technique was able to effectively clear and uniformly label a 1mm-thick block of a mouse brain sample with 86 different antibodies. Thus, the SWITCH protocol seemed feasible for our purposes because the protocol does not require special reagents and was successful in improving the penetration in samples much larger than the *Xenopus laevis* whole brain samples that we work with. Also, unlike CLARITY and ExM, the SWITCH technique had been used to improve the GABA antibody penetration of their sample (Murray et al., 2015), which is the main antibody used for immunolabeling in our experiments. In addition, the protocol also requires the usage of a glutaraldehyde fixative, which could impair IHC efficacy in some systems, but has been used in our regular GABA IHC procedures. Thus, the protocol seemed feasible to incorporate into our methods as a means of improving our GABA IHC.

We thus sought to utilize and incorporate the SWITCH protocol in our methods in order to improve the immunolabeling and visualization of tectal neurons within the complex organization of the *Xenopus laevis* whole brain. We hypothesized that the SWITCH protocol

would be able to improve GABA antibody penetration and allow for uniform labeling in the intact *Xenopus laevis* whole brain once the optimal parameters are established. However, because the technique was mainly performed using whole mouse brains or 1mm-thick blocks of tissue in Murray et al., 2015, which are much larger than *Xenopus* tadpole brains, we experimented with different parameters for each step. Thus, we tested different conditions to establish the appropriate temperatures and incubation times for each step, in order to optimize the technique for the *Xenopus laevis* animal model. Consequently, we performed several variations of the SWITCH protocol in the *Xenopus laevis* whole brain using a GABA antibody, and used confocal microscopy to acquire whole mount images of the brain samples at several depths to analyze the efficacy of the SWITCH protocol in our experiments. A nuclear counterstain was also used to visualize areas where tectal neurons are present to compare whether GABA immunolabeling is also present. We also tested the compatibility of the SWITCH protocol with antibodies for phospho-histone H3 (PH3) and β-tubulin, which have been used to label dividing cells (McKeown et al., 2013) and cellular processes (Liu and Cline, 2016), respectively. Lastly, we evaluated the success of all trials compared to a control sample, where we performed our regular immunohistochemistry procedure in the whole brain.

1.2 Morphological Analyses of Neurons in the *Xenopus laevis* Optic Tectum

One traditional approach to classifying neuronal cell types originates from Ramon y Cajal, who discovered that neuronal morphology was extremely diverse, and that these structural variations may account for different neuronal functions (Ramon y Cajal, 1899). Since then, there have been numerous studies on the differences in morphology between neuronal cell types (Benavides-Piccione et al., 2005; Wang et al., 2018; Kanari et al., 2019). These studies have considered all structural components of the neuron: the soma, dendrites, and axons, and found that different cell types can be distinguished based on their unique morphologies.

Dendritic morphology is an essential component to consider in these analyses because dendrites are sites at which axons may form synaptic contacts, creating the connectivity within neural circuits (Niell et al., 2004). Analyzing differences in dendritic arborization between cells can thus uncover more information about neuronal function and circuit mechanisms (Cline, 2001). The dendritic arborization of a neuron can be described by measuring the number of primary dendrites present, total dendrite branch length, total dendrite branch tip number, dendrite branch density, and dendrite depth, among others. Variations in these dendritic structural attributes may have different functional implications.

Because dendrite length and branching are related to the formation of synaptic contacts, the quantification of these characteristics can be used to compare the functional activities of different neurons. For example, dendritic branch tips have been shown to be sites of synaptic contact (Li et al., 2011). Thus, comparing the total dendrite branch tip number between excitatory and inhibitory neurons may serve as a proxy as to how much synaptic input the neurons are receiving. Total dendrite branch length must also be considered because longer dendrites have more surface area available for these synaptic contacts to be formed. With these attributes quantified, information on the number of primary dendrites and the dendrite branch density for the neurons are made available and can also be compared between excitatory and inhibitory neurons. Measuring the deepest ventral dendrite may also be useful to infer where the neurons are likely receiving input from, as there is lamination within the tectum that distinguishes axonal inputs coming from different brain regions (Hiramoto and Cline, 2009). It has been shown that RGC axons project to the dorsal layers of the tectum (Figure 8A), while hindbrain axons project to the ventral layers (Hiramoto and Cline, 2009). The gap in between these layers may possibly be occupied by axons coming from the contralateral tectum (Gambrill et al., 2016). The comprehensive analyses of these dendritic morphologies to structurally

distinguish between excitatory and inhibitory neurons may thus also lead to the understanding of their functional differences.

Axonal morphology must also be a factor to consider in these analyses as axons are responsible for transmitting synaptic outputs for cellular communication. Thus, axon morphology can be described by total axon length, total axon branch tip number, and axon projection sites, among others. The diversity of these structural properties between excitatory and inhibitory neurons may also be reflective of their functional differences. The total axon branch tip number may exhibit functional importance because axon branches, similarly to dendritic branches, have been shown to be more stabilized sites for synapse formation and maturation (Li et al., 2011). Moreover, the total length of an axon is an important parameter to compare because synapses have been shown to occur all along the length of tectal axons, and not just at their branch tips (Gambrill et al., 2016). Axon projection sites have been used to characterize neuronal cell types in previous studies (Wang et al., 2018; Wang et al., 2019), as this information is necessary to understand which brain regions these neurons are sending output to. Taken together, the quantification of axon morphology may be indicative of the assorted functions of different neuronal cell types.

The cell body, or soma, of a neuron is responsible for the integration of input. Thus, analyzing the different features of somas may also be useful in cell type identification. Specifically, the location of the soma within the brain's lamination may serve as an indicator of neuronal cell types. Observing the position of the neuron's cell body is important for understanding the distribution of cell types across the layering of the brain (Wang et al., 2019). Other studies have also considered the shape and size of the soma, such as surface area and perimeter, to understand how these properties vary across different neuronal cell types (Benavides-Piccione et al., 2006; The Petilla Interneuron Nomenclature Group, 2008; Kanari et

al., 2019). However, these studies have relied on the specific layering of the brain to locate the cell body position. This cell-type specific layering of the brain, although present in the adult frog, is not yet developed in stage 47 *Xenopus laevis* (Lázár, 1973).

Ultimately, the classification of neuronal cell types creates a foundation for understanding how neuronal diversity underlies various brain functions, circuit mechanisms, and behavioral responses (Fishell 2013). A fully comprehensive analysis of neuronal cell types within the optic tectum of the developing *Xenopus laevis* tadpole model has yet to be accomplished. Here we propose to study stage 47 albino *Xenopus laevis* tadpoles to determine whether dendrite and axon morphology can be used to distinguish between excitatory and inhibitory neurons in the optic tectum, which may lead to the future identification of neuronal cell types. Analysis of the soma was not included due to the brain's lamination not being developed at this stage. We hypothesized that dendrite and axon morphology can be used to distinguish between excitatory and inhibitory neuronal cell types within the *Xenopus laevis* optic tectum at stage 47. To test this hypothesis, we transfected neurons in the left tectal lobe in stage 47 albino *Xenopus laevis* using a plasmid to drive GFP expression. We used in vivo and wholemount brain imaging of isolated single GFP-expressing neurons and created reconstructions of their dendritic and axonal morphology. GABA immunolabeling of cross sections was used to classify the cell as inhibitory or excitatory. We then quantified several morphological features to determine whether any significant differences exist between excitatory and inhibitory neurons based on their dendritic and axonal morphology. The dendrite morphological attributes considered include number of primary dendrites, total dendrite length, total dendrite branch tip number, dendrite branch density, and deepest dendrite depth. The axon morphological parameters analyzed include total axon length, total axon branch tip number, and axon projection sites.

MATERIALS AND METHODS

2.1 General Methods

Albino *Xenopus laevis* animal models were obtained from in-house breeding or from Xenopus Express (Brooksville, FL). Animals were reared in a 0.1X Steinberg solution and kept in a 12h light-12h dark cycle at 22°C. Experiments were performed on the tadpoles at Stage 47 (Nieuwkoop and Faber, 1956) of development. Animals were anesthetized using 0.02% tricaine methanesulphonate (MS222) prior to all experiments. All experimental protocols were approved by the Institutional Animal Care and Use Committee of Scripps Research.

2.2 SWITCH Protocol Optimization

We performed the SWITCH protocol (Murray et al., 2015) using the same materials and attempted to optimize this protocol to work for our experiments, which are outlined and further described in Chapter 3.1. The primary antibody used for GABA was a solution of 1:2000 rabbit anti-GABA (A2052; Sigma). The secondary antibody used for GABA was 1:200 donkey anti-rabbit 647 Alexa Fluor (A31573; Invitrogen). The control trial was run the same way as our regular experimental methods described in Chapter 2.3, but the immunohistochemistry was performed on the whole brain rather than sectioned tissue.

All SWITCH and control brain samples are fixed in two rounds of microwave fixation at 150W for 1 minute, and then overnight at 4°C. In our control trial for the phospho-histone H3 (PH3) and β-tubulin samples, we fixed the animal using 4% paraformaldehyde in 1X PBS. The next day, the brains are dissected out and permeabilized in 2% PBST for 1 hour at room temperature. The brains are then quenched in 1% sodium borohydride (NaBH) for 10 minutes at room temperature, and then washed in PBS three times in 1X PBS for 10 minutes each wash. They were then placed in a blocking solution containing 5% normal donkey serum, 2% Triton X-100, in 1X PBS for 1 hour at room temperature. They are then incubated in the blocking solution

in addition to 1:1000 rabbit anti-PH3 antibody (3377S; Cell Signaling Technology) for PH3, or 1:200 mouse anti-β-tubulin antibody (T8535; Sigma-Aldrich) for β-tubulin, for 1 day at 4°C. The samples were then incubated in either 1:200 donkey anti-rabbit 647 Alexa Fluor (A31573; Invitrogen) in 2% PBST for PH3 samples or 1:200 donkey anti-mouse 647 Alexa Fluor (A31571; Invitrogen) in 2% PBST for β-tubulin samples, for 2 hours at room temperature. The samples were then washed three times in 1X PBS, 10 minutes each wash, at room temperature. Lastly they were incubated in 1:10,000 Sytox-O (S11368; ThermoFisher Scientific) in 1X PBS at room temperature for 10 minutes before being mounted in FocusClear (FC-101; Cedarlane), which was used to mount all SWITCH samples onto glass slides.

In Trial #1 (Table 2), the secondary antibodies used for PH3 and β-tubulin were donkey anti-rabbit 488 Alexa Fluor (A21206; Invitrogen) and donkey anti-mouse 647 Alexa Fluor, respectively. In Trial #2 (Table 2), the secondary antibodies used for PH3 and β-tubulin were donkey anti-rabbit 488 Alexa Fluor and donkey anti-mouse 488 Alexa Fluor (A21202; Invitrogen), respectively. For Trial #2 (Table 2), we used 1:3,000 DAPI in 1X PBS for 10 minutes at room temperature as a nuclear stain. For all other trials (Table 2), we used 1:10,000 Sytox-O in 1X PBS for 10 minutes at room temperature as a nuclear stain.

All SWITCH trials were imaged using an Olympus FluoView 500 confocal microscope with an X25 water-immersion lens (1.1 NA). We used the Resonant scanner with Z-correction and 2X averaging to reduce background noise, and a 2X digital zoom. All images were acquired using the Nikon NIS-Elements software.

2.3 Dendrite and Axon Morphology Experiments

We performed single-cell electroporation as outlined in Bestman et al., 2006. We pulled glass filaments (G150F-3; Warner Instruments) to create tip sizes of 2-3μm. An axoporator is used to induce 1ms pulses of -50mV with an ideal resistance of 40MΩ. An oscilloscope is used

to monitor the voltage and ideally records voltages of 0.5-1.5V. We created a mixture of 0.3µL fast green, ddH_2O, and 290-GFP to create 5µL of a 1µg/µL solution of 290-GFP.

Single neurons were targeted in the cell body layer of the left tectal lobe at three different locations and were transfected with plasmid GFP expression using an α-actin promoter (α-actin::GFP). Animals were placed in a bowl of 0.1X Steinberg solution with a bubbler for recovery following electroporation. After 3 days, we screened the animals for isolated single GFP-expressing cells. Only about 10% of the electroporated animals in our experiments yielded imageable single cells. We collected *in vivo* images of the transfected cells using an Olympus FluoView 500 confocal microscope with an X25 water-immersion lens (1.1 NA), and a digital zoom of 1-3X depending on what would show the entire dendritic arborization. We used a Galvano scanner to acquire these images. Images were acquired using Nikon NIS-Elements software. Animals were then anesthetized using 0.02% MS222 solution before being fixed in 4% paraformaldehyde and 2% glutaraldehyde in 1X PBS. The animals were fixed in two rounds of microwave fixation at 150W for 1 minute and then overnight at 4°C.

The brains were then dissected out and quenched in a 1% NaBH solution in PBS for 10 minutes and then washed in PBS for 10 minutes, three times and at room temperature. The brains are then incubated in a 1:3000 DAPI solution for 10 minutes at room temperature to produce a nuclear stain. The brains are then cleared and mounted in a FocusClear (FC-101; Cedarlane) solution, and then imaged whole mount using an Olympus FluoView 500 confocal microscope with an X25 water-immersion lens (1.1 NA). We collected images using a 2X digital zoom with the Resonant scanner and 2X averaging, and used large image acquisition, which involves image stitching by the software, to allow for the entire brain to be included in the image. Resonant scanner was used for whole-mount imaging to speed up the imaging process due to the GABA signal deteriorating in FocusClear after 2 hours. 2X averaging was used to reduce background

noise. These imaging parameters were used to optimize the signal to noise ratio. Images were acquired using Nikon NIS-Elements software.

The brains were then removed from the clearing solution and embedded in a gelatin-albumin mixture for vibratome sectioning into 35µm sections. Sections were then incubated in a blocking and permeabilization solution containing 5% normal donkey serum, 2% Triton X-100 in PBS at room temperature for 1 hour. Sections were then placed in 1:2000 rabbit anti-GABA (A2052; Sigma) in the blocking and permeabilization solution at 4°C for 2-3 days. Sections were then incubated in 1:200 donkey anti-rabbit 647 Alexa Fluor (A31573; Invitrogen) at room temperature for 2 hours. Sections were mounted on glass slides in gel mount (BMDM01; Accurate Chemical & Scientific Corporation) and imaged using 3X digital zoom and Galvano scanner, with 3 channels collected: GFP, DAPI, and GABA Alexa 647.

Dendrites and axons were traced and reconstructed in Imaris (Bitplane) software. Total dendrite branch length, total dendrite branch tip number, total axon length, and total axon branch tip numbers were all quantified in Imaris (Bitplane) software based on the neuronal reconstructions. These methods are depicted in Figure 5.

This section is co-authored with Dang, Vi P. and Faulkner, Regina L. The thesis author was the primary author of this section.

2.4 Statistical Analyses

Microsoft Excel was used for data recording. GraphPad Prism was used for statistical analyses and creating data figures. For normally distributed data, statistical differences between the means of data were calculated using unpaired Student's two-tailed t-tests. For data not normally distributed, statistical differences between the means of data were calculated using a Mann-Whitney test. Chi-squared tests were used to test for statistical differences in data proportions. We report averages as mean±SEM.

RESULTS

3.1 Optimizing the SWITCH protocol in the *Xenopus laevis* animal model

We sought to optimize the published SWITCH protocol to fit our needs for this project: optimal clearing and antibody penetration in the *Xenopus laevis* whole brain without having to section the tissue. We performed the protocol with different adjustments each time in order to produce better penetration and signal of the GABA antibody in the whole *Xenopus* brain. The published protocol uses the parameters as outlined in Murray et al., 2015, but the whole mouse brains or 1mm-thick blocks they used are much larger than our *Xenopus* brain samples, so we adjusted our parameters as necessary.

We set up a control where we performed our regular immunohistochemistry protocol as outlined in Chapter 2.3, but in the whole brain rather than in sectioned tissue, to establish a standard for the penetration efficacy. In our control tissue, there was extremely bright and oversaturated signal seen at the surface of the tissue (Figure 1). Although we are able to see some signal 20-40μm deep, the signal and labeling are not as crisp as in our sectioned tissue samples (Figure 5G). The poor penetration of the GABA antibody was exemplified in that we were not able to observe any labeling in our control sample at 60μm or deeper, which led us to experiment with the SWITCH protocol.

There are several different components of the SWITCH protocol, including the Fix OFF/ON, Fix Inactivation, Thermal Clearing, and Antibody OFF/ON steps. The Fix OFF step allows for fixative to equilibrate and penetrate the entire depth of the tissue while the Fix ON reagent catalyzes the binding of the fixative; this enables uniform fixation throughout the entire tissue. Fix Inactivation is used to remove any unbound fixative molecules still present within the tissue. The Thermal Clearing step is used to wash off the Fix Inactivation reagent and remove lipids from the tissue. The Antibody OFF/ON steps work similarly to the Fix OFF/ON step, but

rather to allow for uniform antibody binding and penetration through the depth of the tissue. Collectively, these steps comprise the SWITCH protocol that has been shown to be effective in overall improvement of uniform fixation and immunolabeling (Murray et al., 2015).

We then performed the protocol exactly as outlined in Murray et al., 2015, and described in Table 1, Trial #1. However, the animals were fixed using 2% glutaraldehyde instead of 1% glutaraldehyde, since we usually use 2% glutaraldehyde to fix the animals. To account for our smaller tissue size compared to the mouse brain used in the original protocol, we also shortened the incubation and wash times as follows: incubation in Fix ON solution for 1 day, washed the samples in PBST for only 4 hours each, incubated samples in Antibody OFF for 2 days, and incubated samples in Antibody ON overnight. DAPI was also used as a nuclear stain to compare with the strength of the GABA signal. We also used FocusClear for the optical clearing instead of their suggested PROTOS mixture because we already had FocusClear in stock and easily accessible. With these parameters, we observed poor signal at the surface of the tissue and only non-specific background signal at 20-40μm that grew dimmer throughout the tissue (Figure 2, Trial #1), which is worse than the results we obtained in our control sample (Figure 1).

For Trials #2-4 we adjusted the incubation time in the Fix OFF and thermal clearing solutions. For Trial #2, we incubated the sample in Fix OFF for only 1 day. This adjustment made no difference in that we still only observed non-specific background signal and no improvement in the GABA antibody penetration or signal. In Trials #3 and #4, we increased the incubation time in the thermal clearing solution to 7 days, since the lipids may not have been entirely removed within 4 days. We incubated samples in Fix OFF for either 1 day in Trial #3 or 2 days in Trial #4. For both Trials #3 and #4, we only observed hazy and indistinct background signal, even at 20μm deep (Figure 2, Trials #3-4), which is even worse GABA antibody penetration and signal than our previous trials.

Considering that we never had an issue with the fixative penetration and uneven fixation of our tissue, we decided to entirely exclude the Fix OFF and Fix ON steps from our procedure. In Trials #5 and #6, we incubated samples in the thermal clearing solution for either 4 days in Trial #5 or 7 days in Trial #6. Again, we only obtained hazy background signal at 20µm deep in Trial #6, and no improvement in the GABA antibody penetration or signal (Figure 2, Trial #6).

In an attempt to reduce the autofluorescence and non-specific background signal, we introduced a quenching step to all future trials using 1% sodium borohydride. We increased the PBST concentration from 0.1% to 1% to improve penetration. We continued to exclude the Fix OFF/ON and Fix Inactivation steps for all trials hereafter, and followed the quenching with incubation in PBST. For Trial #7, we changed the incubation times in the thermal clearing solution and Antibody OFF solution to 2 days and 6 hours, respectively, in case the sodium dodecyl sulfate (SDS)-mediated lipid removal was interfering with the GABA antibody efficacy. With these adjustments, we saw oversaturated signal at the surface, along with extremely poor labeling and mainly non-specific background signal at 20µm deep (Figure 2, Trial #7).

In Trial #8, we used 4% glutaraldehyde in our fixative to align with the amount the SWITCH protocol originally called for, along with the 2 days of thermal clearing and 6 hours of Antibody OFF. We still observed only oversaturated signal at the surface, and no improvement in GABA antibody signal or penetration at 20µm deep (Figure 2, Trial #8). However, when we changed the incubation times in both the thermal clearing solution and Antibody OFF solution to 1 day in Trial #9, we were able to observe clearer GABA signal 20µm deep (Figure 2, Trial #9), which was an improvement from all of our previous attempts, despite the signal becoming less clear at 40µm deep. When we used the same 1 day thermal clearing and Antibody OFF incubation, but with 4% glutaraldehyde fixative in Trial #10, we observed similar results in that there was signaling at 20µm that faded as we got deeper into the tissue at around 40µm (Figure

2, Trial #10). These results indicated that there was no striking difference from increasing the glutaraldehyde concentration of the fixative.

We returned to using our regular fixative solution of 4% paraformaldehyde and 2% glutaraldehyde since there was not a significant impact of changing the glutaraldehyde concentration of the fixative. We continued using a quenching step, and further increased the PBST concentration to 2%, the same concentration used in our standard IHC in sections, in an attempt to increase penetration. In Trial #11, we allowed for 6 hours of thermal clearing and 2 days of Antibody OFF incubation. As a result, we observed oversaturated GABA signal at the surface and poor GABA labeling at 20-40µm (Figure 2, Trial #11). When we skipped the thermal clearing step completely in Trial #12, we observed the same GABA signaling strength (Figure 2, Trial #12) as in Trial #11.

Next, we decided to experiment with different temperatures for the incubations since 37°C is much higher than what our tissue samples are normally exposed to. In Trial #13, our samples were thermally cleared for 1 day, incubated in Antibody OFF for 3 days, and then in Antibody ON for 1 day, all at 37°C. This led to only non-specific background signal observed past the surface (Figure 2, Trial #13). However, when we applied the same thermal clearing and Antibody OFF/ON incubation times but at room temperature in Trial #14, we were able to achieve GABA signal and penetration about 20µm deep (Figure 2, Trial #14), and even some signal at 40µm deep. This suggested that 37°C may be damaging to the *Xenopus* brain tissue, and we decided to move forward using an even lower temperature of 4°C for our Antibody OFF/ON incubations in all future trials.

We next decided to experiment with the temperature and duration of the thermal clearing step. We did thermal clearing at 4°C for Trials #15 and 16, and at 37°C for Trials #17 and #18. In Trial #15, we performed thermal clearing for 1 day at 4°C and observed GABA antibody

penetration and signaling 60-80µm (Figure 2, Trial #15), which was a significant improvement from our previous trials and whole mount control (Figure 1). In Trial #16, we did thermal clearing for 2 days at 4℃, and observed GABA signaling at 40-60µm (Figure 2, Trial #16). In Trial #17, samples were thermally cleared for 1 day at 37℃, which also resulted in GABA signaling at 40-60µm, but not as crisp and widespread (Figure 2, Trial #17 Sample 1). In Trial #18, where samples were thermally cleared for 2 days at 37℃, we were able to see better and more widespread GABA signaling at 40-60µm (Figure 2, Trial #18). However, there was more variation and inconsistency in results from samples cleared at 37℃. For example, although there was crisp signal observed in one of the samples from Trial #17 (Figure 2, Trial #17 Sample 1), another sample that was incubated in the same tube, and thus experienced the same conditions, showed poorer signaling within the same depths (Figure 2, Trial #17 Sample 2). The samples thermally cleared at 4℃ thus displayed more consistent results and more uniform GABA signaling throughout the depth of the tissue.

Since we established that the thermal clearing worked better at 4℃, we next decided to experiment with more significant changes in the duration of Antibody OFF incubations. Samples were incubated in Antibody OFF at 4℃ for either 3 days in Trial #19 or 7 days in Trial #20. Surprisingly, we saw similar results for both sets of samples: mostly non-specific background signal and some GABA signal at the surface of the tissue (Figure 2, Trials #19-20) near where the tissue had been accidentally torn during dissection. These results were much worse than what had been previously observed in all other trials.

Next, we performed our IHC according to our control protocol while also utilizing the thermal clearing step of the SWITCH protocol. In Trial #21, we performed thermal clearing, followed by our regular primary and secondary antibody steps as outlined in Chapter 2.3. After 1 day of thermal clearing at 37℃ and using the regular primary and secondary antibody methods,

we were able to see some GABA signal 20μm deep (Figure 2, Trial #21), but nothing past that. We therefore concluded that although the SWITCH protocol was able to improve the GABA signaling compared to our control in some trials (Figure 2, Trials #9-10, 14-18), it was not successful enough to reach the entire 60-100μm depth needed to visualize immunolabeled cells in the intact optic tectum.

Because of the variable inconsistent results and none of the parameters working to our advantage to improve GABA antibody penetration throughout the entire tissue, we decided to test the SWITCH protocol using phospho-histone H3 (PH3) and B-tubulin antibodies in case it was the GABA antibody that was incompatible with the protocol. We used PH3 antibodies to label mitotic cells in proliferative zones, and β-tubulin antibodies to label neuronal processes in the *Xenopus* whole-mount brain, with Trials #1-4 described in Table 2.

We first set up a control group and used the experimental methods described in Chapter 2.2. Based on the results of our controls, we found that PH3 already expresses strong signal and penetration depth (Figure 3), so we experimented with SWITCH to see if it would improve or worsen the PH3 immunolabeling. On the other hand, β-tubulin immunolabeling has previously been used and efficient only in sectioned tissue (Liu and Cline, 2016), and thus in our control trial using the whole mount brain, we observed poor antibody penetration and signal only at the surface of the tissue (Figure 3). Therefore, we experimented with SWITCH to see if it would improve β-tubulin antibody signal and penetration in the whole mount *Xenopus* brain.

In our first trial, we used 4% paraformaldehyde as a fixative, since this was usually used when immunolabeling with PH3 and β-tubulin to avoid glutaraldehyde interference with the antibodies' efficacy. We first tested to see if temperature differences would affect the antibodies' signal and penetration, and compared the results of performing the SWITCH protocol at either 4°C in Trial #1 or 37°C in Trial #2. We were able to obtain efficient PH3 signal and penetration

for both trials and temperatures all throughout the tissue (Figure 4, PH3 Trial #1-2); these results did not differ much from the control sample. For the β-tubulin Trial #1 sample at 4℃, we observed only some hazy and indistinct labeling at 20-40μm (Figure 4, β-tubulin Trial #1). The β-tubulin Trial #2 sample that was incubated at 37℃ was lost during processing, and the higher temperature may have contributed to the disintegration of the tissue, making the sample much more fragile and difficult to work with.

In order to maintain the structural integrity of the tissue samples at 37℃, in Trial #3 we decided to add 2% glutaraldehyde to the fixative. We found that although the tissue was more stabilized in structure, the PH3 signal was not as strong throughout the depth of the tissue (Figure 4, PH3 Trial #3) as it was when only paraformaldehyde fixative was used. The β-tubulin sample also maintained its structure, yet also showed only non-specific background signal and poor antibody penetration throughout the entire tissue (Figure 4, β-tubulin Trial #3). We attributed the hampering of the signal to the glutaraldehyde interfering with the PH3 antibody, and thus returned to using only 4% paraformaldehyde as a fixative.

Lastly, to see if thermal clearing alone would affect antibody signal and penetration, we decided to perform only the clearing step of the SWITCH protocol in Trial #4. The tissue was thermally cleared at 4℃ for 2 days, followed by our regular primary and secondary antibody steps as outlined in Chapter 2.2. As a result, we observed consistent PH3 antibody signal throughout the entire tissue (Figure 4, PH3 Trial #4), with no improvement or diminishment from what we initially observed in our control. For the β-tubulin sample, there was still poor antibody penetration and no improvement in signal in the entire tissue (Figure 4, β-tubulin Trial #4). Overall, the SWITCH protocol did not improve the antibody penetration or signal in the whole-mount *Xenopus* brain in our experiments even with PH3 and β-tubulin antibodies.

3.2 Analysis and comparison of dendritic morphology

Dendrites are sites for synaptic contact and thus are responsible for receiving and integrating input information from axons. To understand whether there are differences in the amount of information that may be received and integrated, we analyzed and compared several morphological features of dendrites between excitatory and inhibitory tectal neurons (Figure 5), including number of primary dendrites, total dendrite branch length, total dendrite branch tip number, dendrite branch density, and deepest dendritic point. A total of 37 tectal neurons were analyzed, of which 28 were excitatory and 9 were inhibitory (Figure 6). This unequal ratio of excitatory and inhibitory neurons acquired and analyzed reflects the fact that only 30% of neurons in the optic tectum are GABAergic (Miraucourt et al., 2012).

The primary dendrites of a neuron are the dendrites that emerge directly from the cell body. The number of primary dendrites was analyzed and compared between excitatory and inhibitory tectal neurons. Both groups had similar numbers of primary dendrites (Figure 7A), as excitatory neurons had 2.39 ± 0.24 primary dendrites and inhibitory neurons had 1.89 ± 0.35 primary dendrites ($p=0.2546$).

The total dendrite length of a neuron is telling of how much information may be received by a dendrite because longer length means more surface area available for synaptic contact. To observe whether there were any differences in the total dendrite lengths of excitatory and inhibitory tectal neurons, we quantified the total dendrite length in Imaris (bitplane) based on the live image dendritic reconstruction (Figure 5C-D). We then analyzed and compared the average values between excitatory and inhibitory neurons (Figure 7B). The total dendrite lengths of excitatory neurons had a larger range of 566 - 2216µm, while inhibitory neurons' total dendrite length ranged between 752 - 1475µm. Despite this difference in range, excitatory and inhibitory neurons exhibited similar average total dendrite branch lengths of 1373 ± 80.80µm and 1071 ±

74.42μm (p=0.051), respectively. However, since the p-value is very close to being p<0.05, it suggests that the difference in total dendrite length between excitatory and inhibitory tectal neurons may become significant with a larger sample size.

Dendrite branch tips are stabilized sites of synaptic contact (Li et al., 2011), allowing for input information to be processed and integrated by the neuron. Thus, analyzing the number of dendrite branch tips serves as a proxy for the number of synapses being made onto the cell, which translates to how much information a cell receives. To determine whether excitatory and inhibitory neurons in the optic tectum differed in their total dendritic branch tip number, we quantified the number of branch tips in Imaris (bitplane) based on the live image dendritic reconstructions (Figure 5C-D). Comparing these values (Figure 7C), excitatory neurons had a larger range in number of branch tips (22 - 240 branch tips) than inhibitory neurons (20 - 134 branch tips). On average, excitatory neurons had a significantly greater number of dendrite branch tips (131.1 ± 10.34 branch tips) than inhibitory neurons (74.56 ± 12.76 branch tips, p=0.007).

With the information on the total dendrite length and total number of dendrite branch tips available, we were also able to measure and compare the dendrite branch density per 100μm for all cells (Figure 7d). We used the following formula to compute the dendrite branch density values:

$$Dendrite\ Branch\ Density\ = \frac{Total\ Dendrite\ Branch\ Tip\ Numbers}{Total\ Dendrite\ Length\ (\mu m)} \times 100$$

We found that excitatory neurons have a significantly greater dendrite branch density (9.43 ± 0.45 branch tips/100μm) than inhibitory neurons (6.703 ± 0.89 branch tips/100μm) in the optic tectum (p=0.007). This was expected because excitatory neurons were found to have a greater number of total dendrite branch tips than inhibitory neurons, but both groups of neurons were not significantly different in their total dendrite lengths.

Understanding the depth of the dendrites is important as it may suggest where cells are receiving input from since the lamination within the tectum distinguishes axonal inputs (Hiramoto and Cline, 2009) coming from different brain regions (Figure 8A). To investigate any differences in the deepest dendrite point for excitatory and inhibitory tectal neurons, we measured the deepest ventral dendrite point in Imaris (bitplane) by rotating the live image dendritic reconstruction onto the XZ plane and recording the dendrite's deepest Z coordinate (Figure 8B-C). We then compared these points between both groups (Figure 8D), and found that inhibitory and excitatory neurons extended dendrites to similar depths. Excitatory and inhibitory neurons had average depths of 99.04 ± 6.22μm and 108.2 ± 15.91μm ($p=0.522$), respectively. Unlike the other dendritic characteristics measured, excitatory and inhibitory neurons were also similar in their ranges of depth values, which were 62 - 176μm and 56 - 209.5μm respectively.

3.3 Analysis and comparison of axonal morphology and projections

Axons facilitate cellular communication in a circuit by transmitting output information through synapses. Therefore, the axonal characteristics of a cell may depict how much information is being communicated and transmitted from the cell. We thus analyzed and compared the total axon length, total axon branch tip number, and axon projection sites of excitatory and inhibitory neurons in the optic tectum to investigate whether they differed in axonal properties. We analyzed a total of 39 tectal neurons, with 30 being excitatory and 9 being inhibitory (Figure 10).

The length of an axon may be directly related to the amount of synapses a cell is making since synapses have been found to form all along the length of tectal axons (Gambrill et al., 2016). In order to understand whether excitatory and inhibitory tectal neurons differed in their total axon lengths, we measured the axon lengths in Imaris (bitplane) using the whole-mount image axonal reconstruction (Figure 5E-F). When comparing axon lengths between excitatory

and inhibitory neurons (Figure 9A), excitatory neurons had an average axon length of 2352 ± 156.3μm, which was not significantly different from the average inhibitory axon length of 1907 ± 446.5μm, ($p=0.240$).

Axon branch tips contain stabilized axon terminals that are involved in forming synapses (Li et al., 2011). Thus, the number of branch tips an axon has is directly related to the amount of synapses the cell makes to facilitate cellular communication. We therefore quantified the number of axon branch tips of each cell in Imaris (bitplane) using the whole-mount image axonal reconstruction (Figure 5E-F) to observe whether there were any differences in axon branch tip number between excitatory and inhibitory tectal neurons. Excitatory and inhibitory neurons had almost the same average number of axon branch tips, which were 24.2 ± 2.29 branch tips and 26.67 ± 4.78 branch tips ($p=0.619$), respectively (Figure 9B).

Analyzing axon projection targets is indicative of what brain regions a neuron is communicating with and sending information to. To identify any differences in the axon projection sites between excitatory and inhibitory neurons, we noted the brain region where each axon terminal was located based on the whole-mount image axonal reconstruction. The brain regions analyzed were the contralateral and ipsilateral thalamus, tectum, tegmentum, and hindbrain (Figure 10). We compared the number of cells with axon terminals in each of these target locations (Figure 11A) and observed a higher number of excitatory axons projecting to the ipsilateral hindbrain. Specifically, 83.3% of the excitatory neurons analyzed had axons projecting to the ipsilateral hindbrain, as opposed to only 44.4% of inhibitory neurons analyzed having these projections, ($p=0.019$). The proportion of excitatory and inhibitory neurons projecting to all other brain regions was similar.

For each cell, we also calculated the proportion of axon branch tips that are located in each of the target regions (Figure 11B), using the formula:

$$Proportion\ of\ Axon\ Branch\ Tips\ per\ Target\ Location\ =$$

$$\frac{Number\ of\ Axon\ Branch\ Tips\ of\ Cell\ in\ Target\ Location}{Total\ Number\ of\ Axon\ Branch\ Tips\ of\ Cell}$$

This formula also accounts for cells that do not contain any axon branch tips in each of the target locations. We found that excitatory and inhibitory neurons had similar proportions of their axon branch tips in each of the target locations, with the exception of the ipsilateral hindbrain. Excitatory neurons had a greater proportion (0.155 ± 0.028) of their axon branch tips in the ipsilateral hindbrain, as opposed to inhibitory neurons (0.023 ± 0.01), which was significantly different (p=0.002).

We also measured the number of axon branch tips in each of these brain regions and compared the average values between excitatory and inhibitory tectal neurons (Figure 11C). The average value of axon branch tips in each target location was calculated using the formula:

$$Average\ Axon\ Branch\ Tip\ Number\ =$$

$$\frac{Total\ number\ of\ axon\ branch\ tips\ in\ target}{Number\ of\ cells\ with\ axon\ projections\ in\ target}$$

In contrast to the proportion of axon branch tips per target location, this formula only accounts for the neurons that project to these regions, and excludes neurons which have 0 branch tips in these locations. Most of the brain regions analyzed had similar average numbers of axon branch tips between excitatory and inhibitory tectal neurons. However, there was a significantly greater number of inhibitory axon branch tips in the contralateral tectum, 6.33 ± 1.86 branch tips, than excitatory axon branch tips, 2.17 ± 0.48 branch tips (p=0.048), despite similar amounts of excitatory and inhibitory cells projecting there.

This section is co-authored with Dang, Vi P. and Faulkner, Regina L. The thesis author was the primary author of this section.

DISCUSSION

Our experimentation with the SWITCH protocol was not entirely successful in improving the GABA antibody signal and penetration in the developing *Xenopus laevis* animal model, despite the protocol having profound success in the mouse whole brain (Murray et al., 2015). Surprisingly, although Murray et al., 2015 had successfully tested the protocol using a GABA antibody, the GABA antibody signal and penetration only improved in Trials #9-10 and #14-18 of our experiments (Figure 2). Even the success in these trials was limited as 80μm (Figure 2 Trial #15) was the maximum antibody penetration depth achieved, which is not deep enough to reach the entire depth of the whole *Xenopus* brain.

Although we were able to achieve some improvements with GABA antibody penetration, we were not as successful with antibodies for PH3 and β-tubulin. For the β-tubulin samples, we observed minimal improvement in antibody penetration only when performing the protocol at 4°C (Figure 4 Trial #1). For PH3, there was not much improvement needed as the labeling works efficiently throughout the entire depth of the tissue in our control (Figure 3). However, we did notice that the immunolabeling diminished when glutaraldehyde was used in the fixative, which suggests that glutaraldehyde hampers the efficacy of the PH3 antibody. These results were surprising since these antibodies were also tested in the original SWITCH experiments by Murray et al., 2015.

We concluded that the SWITCH protocol was inefficient in improving the antibody penetration in our experiments, even though we performed the tests using the same conditions and antibodies as presented in the original protocol (Murray et al., 2015). This suggests that the failures of our trials may be attributed to the incompatibility of the SWITCH protocol with the *Xenopus laevis* brain and tissue composition. Murray et al., 2015 performed the protocol using mouse and human tissue, which may be different in molecular and structural composition from

Xenopus tissue. This is supported in that the mouse brain samples were able to maintain their structural integrity under the conditions and temperatures required in the SWITCH protocol (Murray et al., 2015), while the *Xenopus* brain samples became very fragile or even disintegrated when incubated at 37℃. This increased fragility and sensitivity made it difficult to handle the *Xenopus* samples at higher temperatures, which led to the loss of some samples during processing. This explains why we observed more improvement in antibody penetration when performing the protocol at 4℃ (Figure 2 Trial #15; Figure 4 β-tubulin Trial #1), a temperature at which the samples are usually contained.

Another possible explanation for the inefficiency of the SWITCH protocol in our experiments is that the incompatibility of the protocol with our samples and materials is multifaceted. SWITCH operates on the basis of a tightly controlled operation of time and chemical kinetics (Murray et al., 2015). This suggests that with these specific conditions, such as the 37℃ temperature used, are crucial for the efficacy of the protocol and full antibody penetration throughout the entire depth of the mouse brain. However, since the *Xenopus* brain sample is not able to withstand the 37℃ condition, 4℃ worked better in favor of our experiments since we were able to improve the GABA and β-tubulin antibody penetration in trials done at 4℃ (Figure 2 Trial #15; Figure 4 β-tubulin Trial #1). Despite this achievement, the antibody was still not able to fully penetrate the entire depth of the whole *Xenopus* brain. Meanwhile, the GABA and β-tubulin antibody tested in Murray et al., 2015 was able to penetrate the entire mouse brain sample, which is much larger than the *Xenopus* brain. This inconsistency in results could be explained by an incompatibility between the antibody, temperature, and structural integrity of the sample. Perhaps 4℃ works better to maintain the structural integrity of the *Xenopus* brain sample, but 37℃ may be the temperature required to allow for full efficacy and penetration of the GABA and β-tubulin antibody. In addition, the SWITCH protocol requires

the usage of glutaraldehyde as a fixative to maintain the sample under these higher temperatures, but glutaraldehyde hinders the efficacy of the PH3 and β-tubulin antibodies (Figure 4 Trial #3). Therefore, these complex relationships and interactions between the materials and conditions involved may have led to the ineffectiveness of the SWITCH protocol in our experiments.

Moving forward with our experiments using our regular protocol, our morphological analyses partially supported our hypothesis that dendrite and axon morphology may be distinguishing characteristics of excitatory and inhibitory neurons in the optic tectum of stage 47 albino *Xenopus laevis.* We found that only some characteristics of dendrite and axon morphology may be unique between excitatory and inhibitory neurons, including total dendrite branch tip number, dendrite branch density, and axon projection sites.

Regarding dendritic morphology, excitatory neurons were found to have a greater amount of total dendrite branch tip numbers (Figure 7C), and thus a greater dendrite branch density (Figure 7D), than inhibitory neurons in the optic tectum. This suggests that excitatory tectal neurons receive more input since they contain more stabilized sites of synaptic contact (Li et al., 2011). This also conflicts with the findings by He et al., 2016 that excitatory and inhibitory tectal neurons are similar in their total dendrite branch tip numbers and thus cannot be distinguished by their dendritic arborization. This may be explained by the difference in developmental stages analyzed; He et al., 2016 performed electroporation at stage 44-45 before analysis at stage 47, while we electroporated our animals at stage 47 and thus analyzed neurons even later in development. Therefore, the findings in He et al., 2016 may be true for more immature neurons, rather than at the more mature stages we studied here.

In all other aspects of dendrite morphology, excitatory and inhibitory tectal neurons were found to be more similar. The similarity in number of primary dendrites coincides with findings that the number of primary dendrites was not significant for defining cell types in mice

(Benavides-Piccione et al., 2006). Their similarity in dendrite length conflicts with the usage of dendrite length as a distinguishing characteristic of neuronal cell types in mice (Benavides-Piccione et al., 2006). However, our p-value was very close to being significant (Figure 7B), which indicates that this dendritic parameter may become significant with a larger sample size. The similarity in deepest dendrite depths between excitatory and inhibitory tectal neurons suggests that they may be receiving input via axons of similar origins.

In terms of axon projection sites of tectal neurons, we observed more excitatory neurons with axons projecting to the ipsilateral hindbrain (Figure 11A), a higher proportion of excitatory axon branch tips in the ipsilateral hindbrain (Figure 11B), and a higher average of inhibitory axon branch tips in the contralateral tectum (Figure 11C). These findings support the use of axon projections as parameters to distinguish between neuronal cell types in various animal models (Tasic et al., 2016; Tasic et al., 2018; Wang et al., 2018; Wang et al., 2019). The increased excitatory axon projections to the hindbrain suggest that there is more excitatory communication occurring between neurons of the tectum and the ipsilateral hindbrain, within the retinotectal circuit. There also may be more excitatory synapses forming in the hindbrain, as the higher amount of excitatory axon branch tips indicates a higher amount of stabilized sites of synaptic contact (Li et al., 2011). As for the greater average amount of inhibitory axon branch tips in the contralateral tectum, this finding suggests that the balance of excitation and inhibition within the tectal circuit is maintained by an increased number of inhibitory axon branch tips. Thus, although only 30% of the tectal neurons are GABAergic (Miraucourt et al., 2012), the level of inhibition within the intertectal circuit may be regulated by increased number of inhibitory axon branch tips.

Other aspects of axon morphology analyzed, including total axon length and total number of axon branch tips, were found to be similar between excitatory and inhibitory neurons in the

optic tectum. These results suggest that excitatory and inhibitory tectal neurons are sending information to similar target regions and are overall forming similar amounts of synapses. This contradicts the usage of axon length and branch tip number as a distinct signifier of pyramidal cell types in the somatosensory cortex of rats (Wang et al., 2018). However, the conflicting significance of axon length and branching as a defining characteristic of cell types may simply be a consequence of variation in neuronal structure across different animal models. Because rats are mammals and more complex in nature, their neurons may be further distinguished by their axonal characteristics, unlike in our more simple *Xenopus* animal model.

This was the first concerted effort to create a comprehensive analysis of neuronal cell types in the optic tectum of stage 47 *Xenopus laevis*. Though we were able to pinpoint several morphological characteristics that distinguished excitatory and inhibitory neurons, there is much more to be considered, such as the tortuosity and volume of these features (Wang et al., 2018). Our results also suggest that further investigation of axon projection sites is necessary to probe for a better understanding of the regions involved in communication in the tectal circuit. In addition, it would be interesting to incorporate the neurons' experience-dependent structural and functional plasticity, or plasticity profile (He et al., 2016), in future studies to observe whether their differences in plasticity are maintained in the more mature stages studied here. This could potentially unveil a relationship between their plasticity profiles and differences in morphology, linking the structural and functional properties of these neuronal cell types. Future studies should also seek to improve the success of acquiring single transfected neurons in order to collect data from a larger sample size. Thus, the wiring and mechanisms of the retinotectal circuit that facilitate different behavioral responses remains to be further explored in the developing *Xenopus* model.

Useful applications of these analyses includes the compilation of data from all neurons to create a comprehensive database of cell types in the *Xenopus* brain, as done in the *Drosophila* model (Chiang et al, 2011). These databases may be used as a resource to study the properties and connectivity between different cell types in the brain. Furthermore, this would enable researchers to understand how neural circuitry underlies behavior, development, and disease.

FIGURES AND TABLES

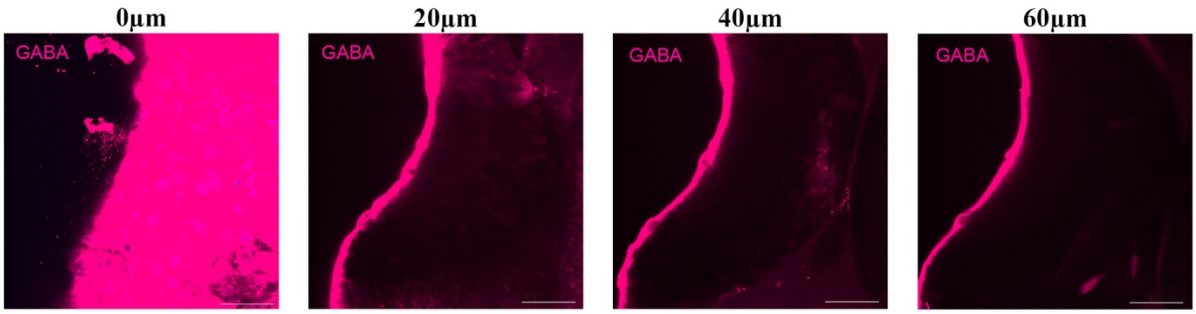

Figure 1. Images of the left tectal lobe after performing GABA immunohistochemistry in the Xenopus laevis whole brain using our regular protocol as a control. GABA+ cell bodies are shown as opaque pink cells, while GABA- cell bodies are shown as hollow black cells. A 2X optical zoom was used for all images. The depths at the top of each image represent the depth in the *Xenopus* whole brain at which the image was acquired. Scale bar represents 50µm.

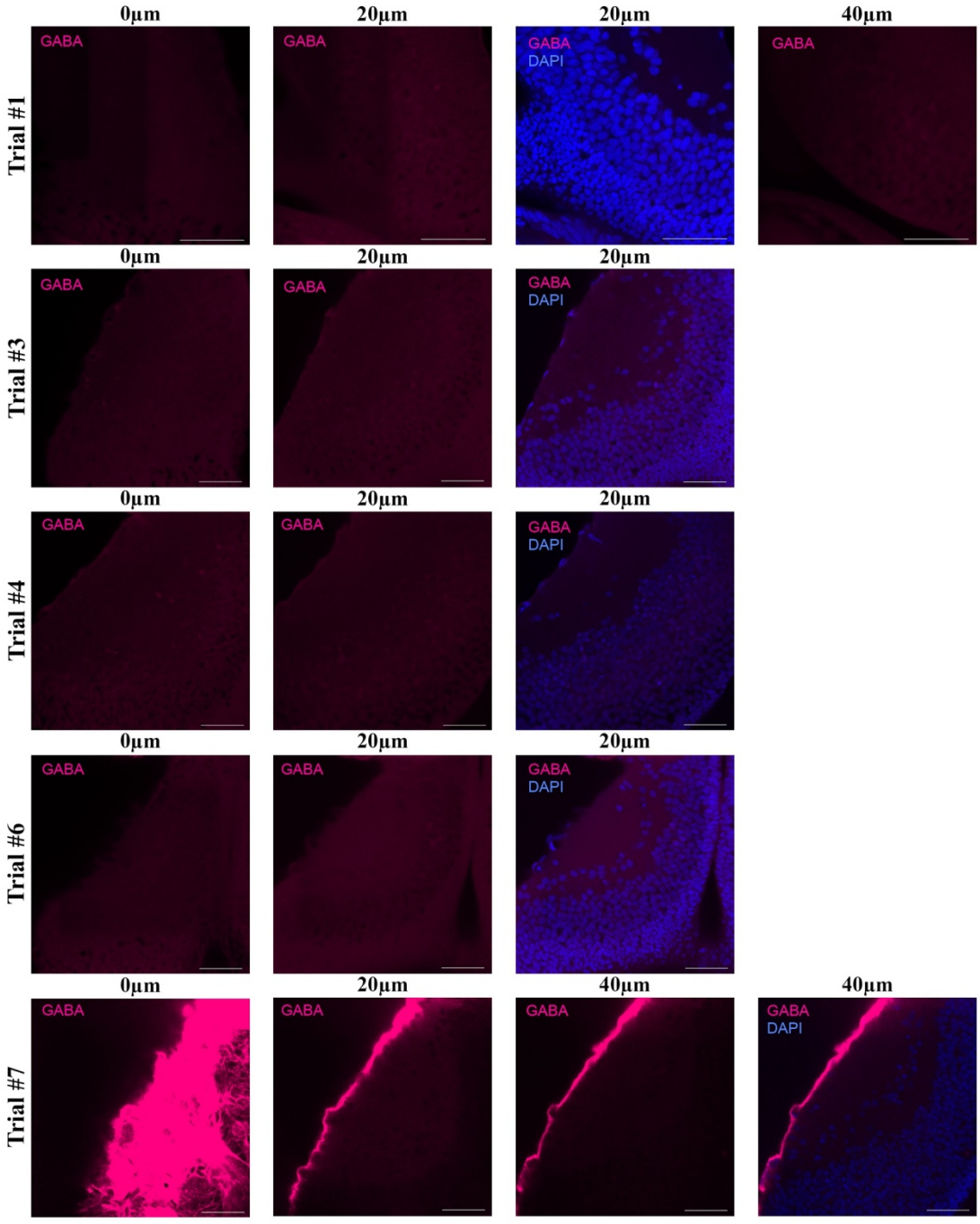

Figure 2. Images of the tectal lobe after performing GABA immunohistochemistry in the Xenopus laevis whole brain using several variations of the SWITCH protocol. GABA (pink) stains GABAergic cell bodies, and DAPI (blue) was used as a nuclear stain. Trial numbers correspond to those in Table 1. Images of Trials #1, #10, #14, and #18 show the right tectal lobe. The left tectal lobe is pictured in all other trials. The depths at the top of each image represent the depth in the *Xenopus* whole brain at which the image was acquired. Scale bar represents 50µm.

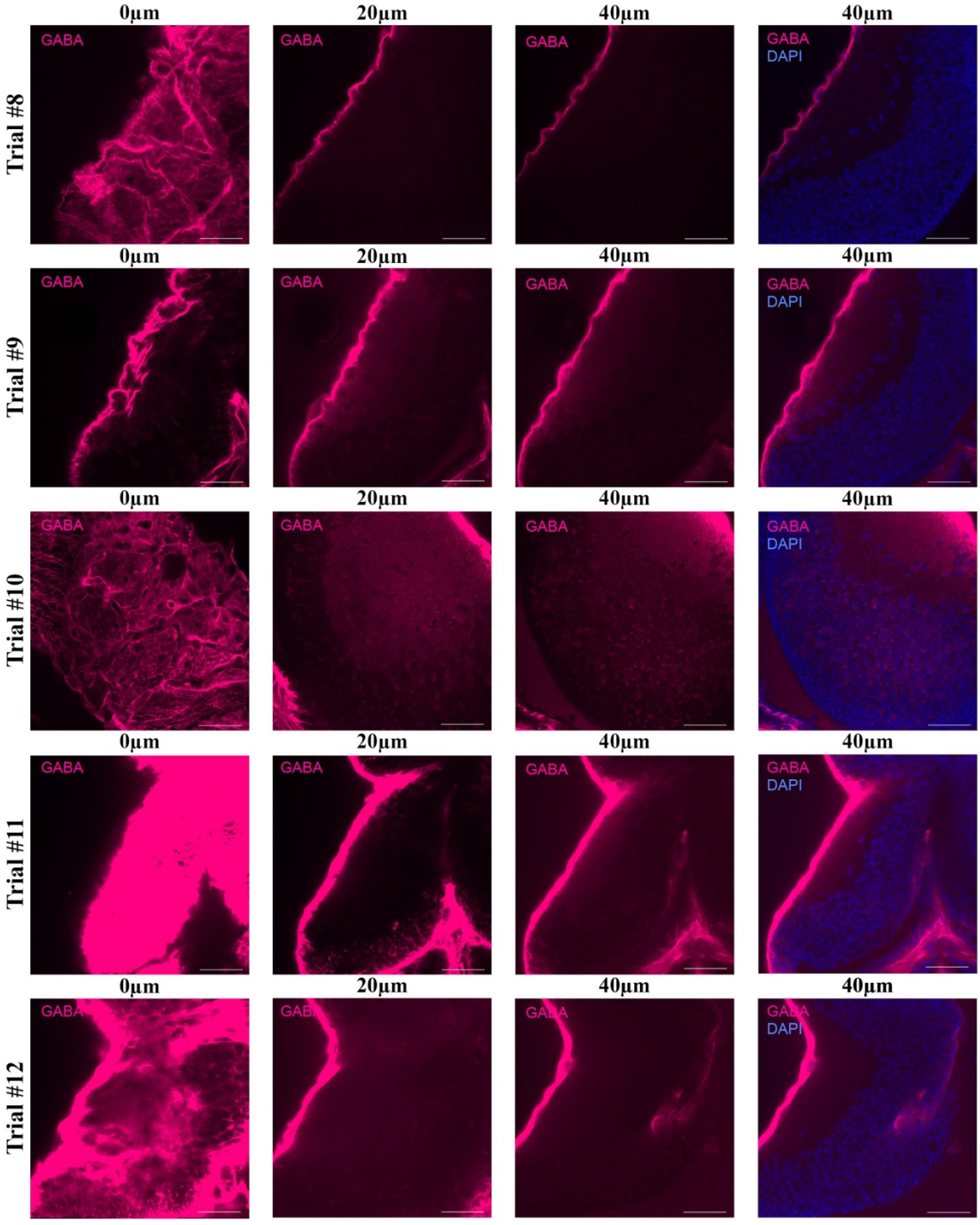

Figure 2. Images of the tectal lobe after performing GABA immunohistochemistry in the *Xenopus laevis* whole brain using several variations of the SWITCH protocol, continued.

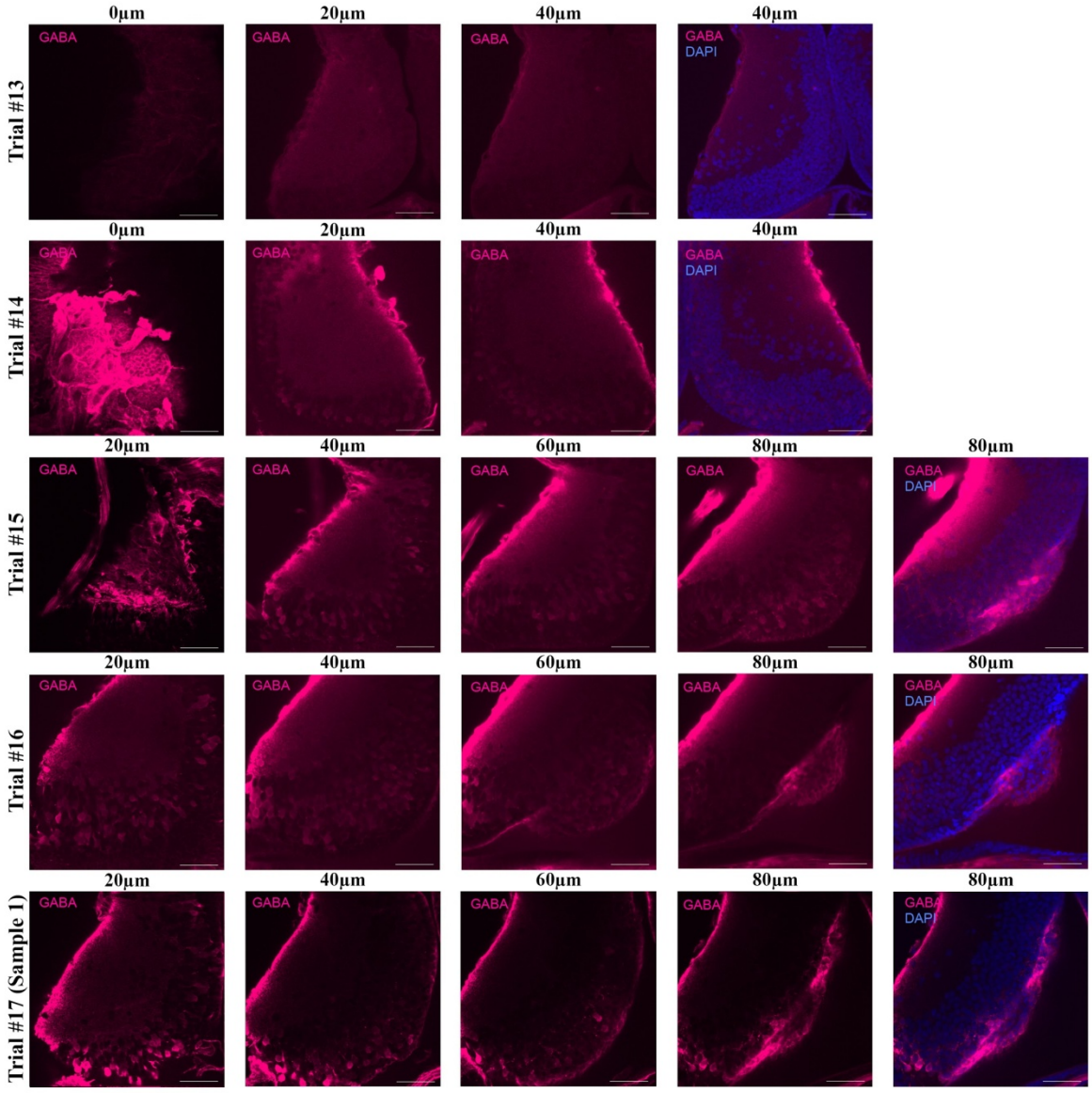

Figure 2. Images of the tectal lobe after performing GABA immunohistochemistry in the *Xenopus laevis* whole brain using several variations of the SWITCH protocol, continued.

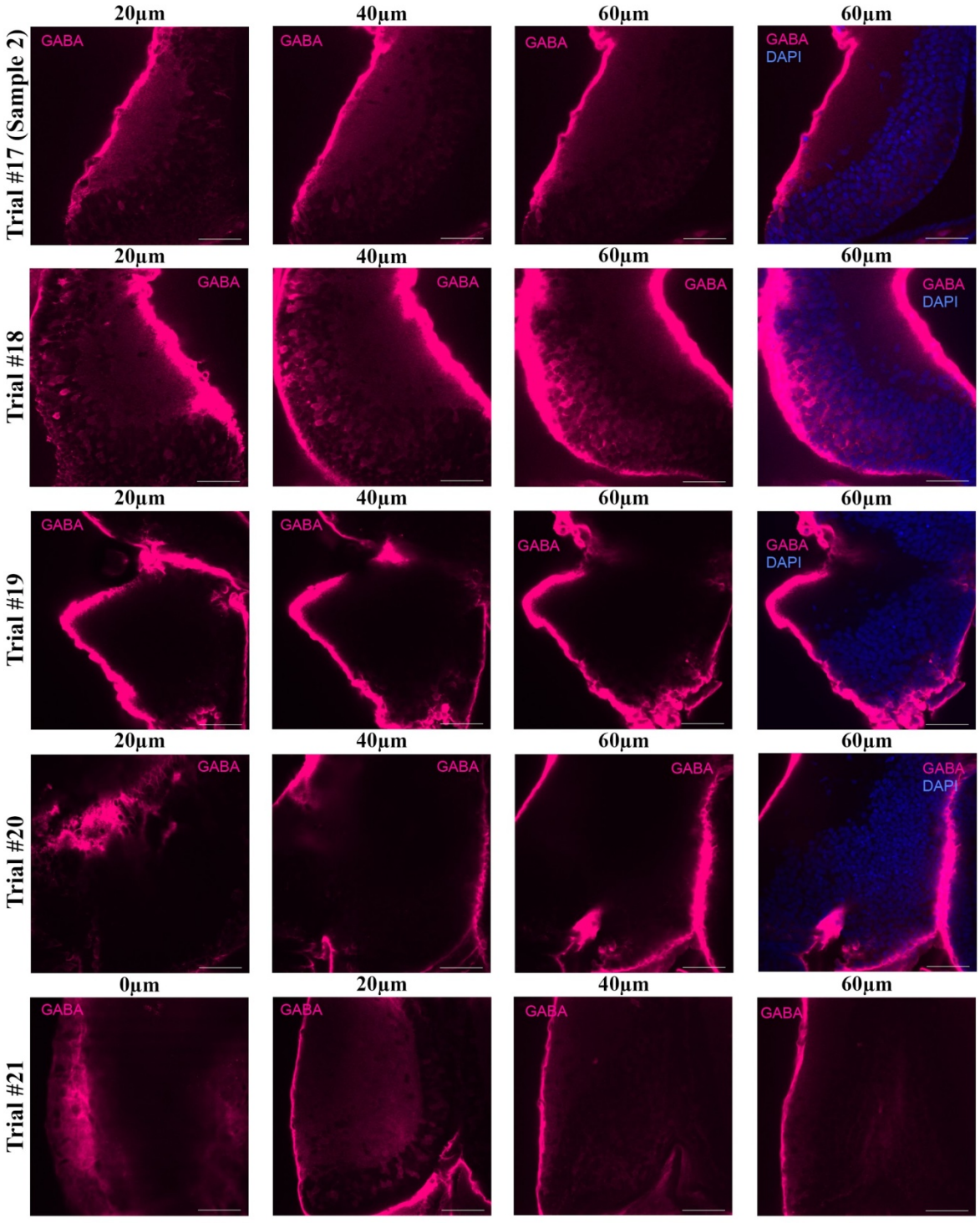

Figure 2. Images of the tectal lobe after performing GABA immunohistochemistry in the *Xenopus laevis* whole brain using several variations of the SWITCH protocol, continued.

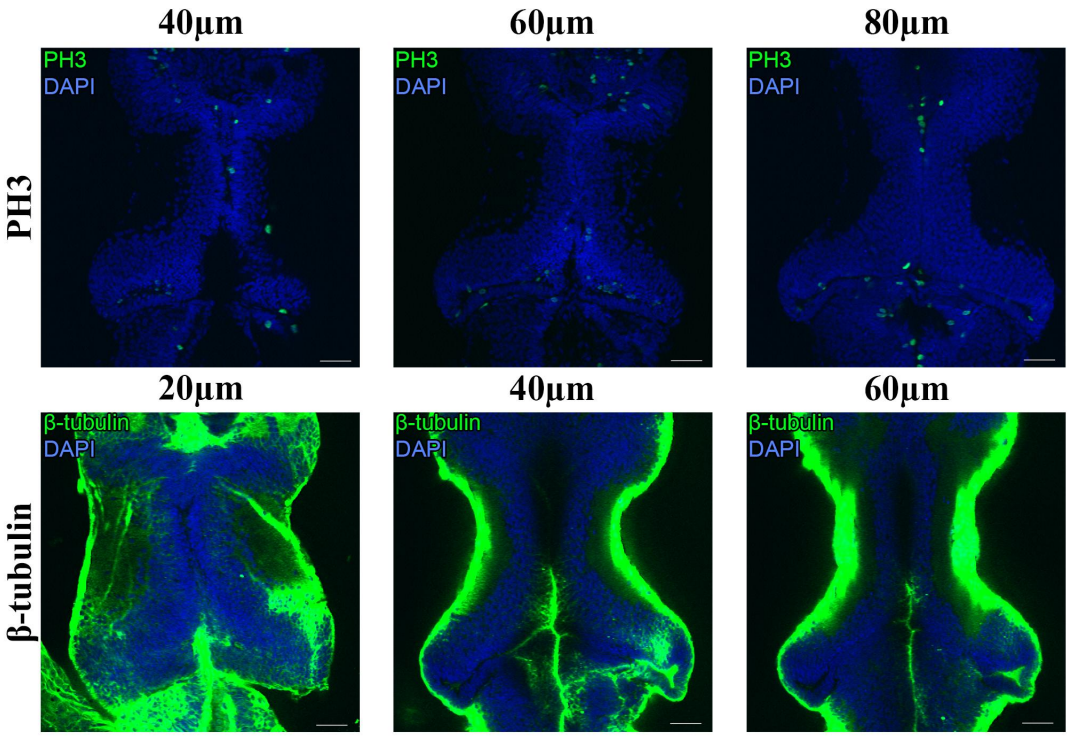

Figure 3. Images of the optic tectum after performing PH3 and β-tubulin immunohistochemistry in the Xenopus laevis whole brain using our regular protocol as a control. PH3 (top) labels dividing cells and β-tubulin (bottom) labels neuronal processes. DAPI (blue) was used as a nuclear stain for both groups. The depths at the top of each image represent the depth in the *Xenopus* whole brain at which the image was acquired. Scale bar represents 50µm.

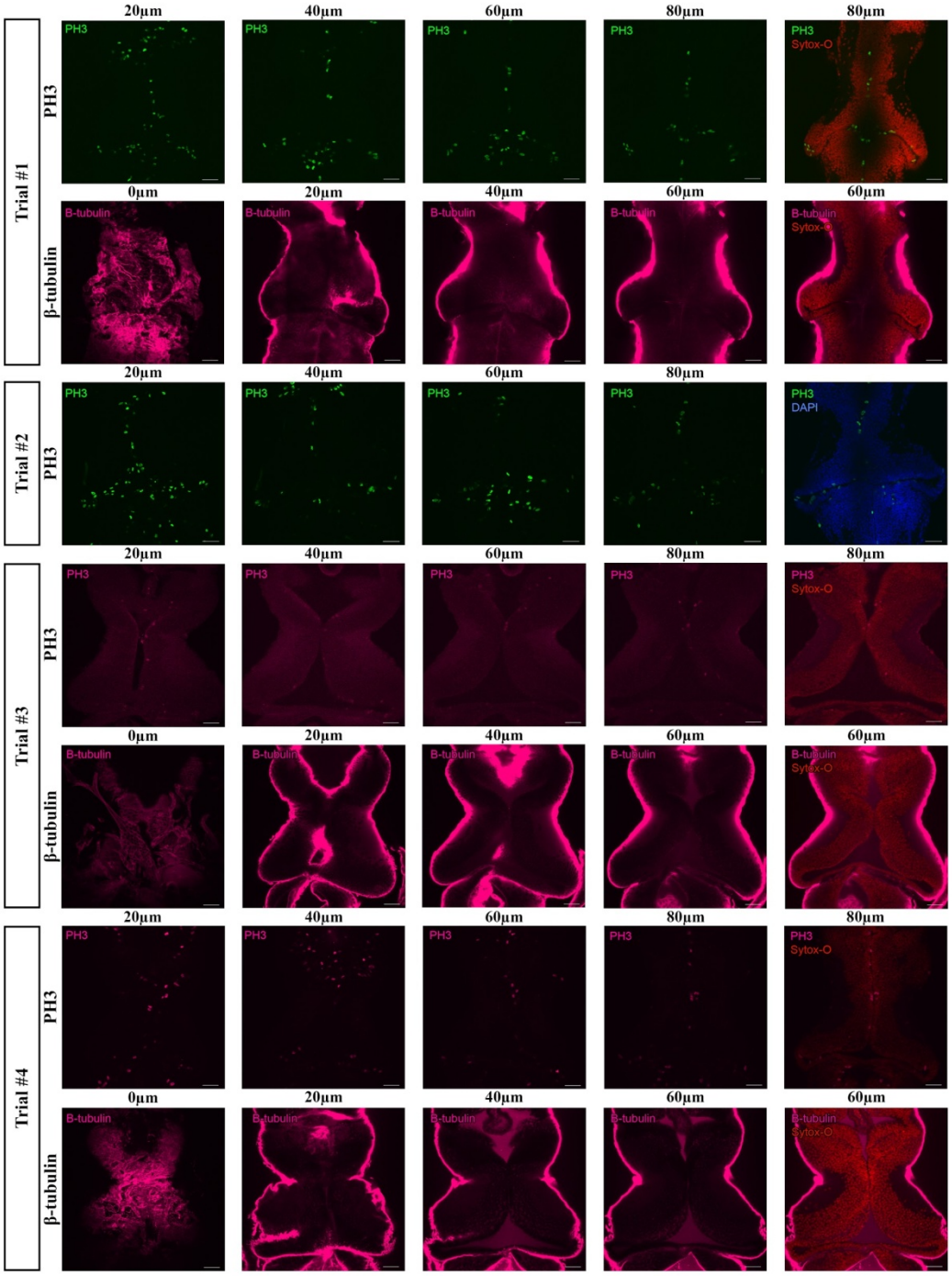

Figure 4. Images of the optic tectum after performing PH3 and β-tubulin immunohistochemistry in the Xenopus laevis whole brain using several variations of the SWITCH protocol. PH3 labels dividing cells and β-tubulin labels neuronal processes. DAPI (blue) was used as a nuclear stain. Trial numbers correspond to those in Table 2. Sample of Trial #2 of β-tubulin was lost during processing, and thus is not shown.The depths at the top of each image represent the depth in the *Xenopus* whole brain at which the image was acquired. Scale bar represents 50µm.

Figure 5. Depiction of the methods and workflow used for morphological analyses of neurons in the Xenopus laevis optic tectum. (A) Flowchart depicting the methods used for morphological analyses of neurons in the *Xenopus laevis* optic tectum. (B) Dorsal schematic of the *Xenopus laevis* and the single-cell electroporation technique. Single neurons in the left tectal lobe of stage 47 *Xenopus* tadpoles were targeted with a plasmid driving GFP expression (α-actin::GFP). (C) Live image of a single GFP+ neuron in the left tectal lobe of the *Xenopus laevis*. A 2.5X optical zoom was used. Scale bar represents 50µm. (D) Dendritic reconstruction based on the live image and neuron in part C. (E) Image of the whole mount brain of the *Xenopus laevis* with an axonal reconstruction overlay of the neuron in part C. A 2X optical zoom was used with image stitching. Scale bar represents 50µm. (F) Schematic of the entire *Xenopus laevis* brain, overlay with the axonal reconstruction of the neuron based on the whole mount image in part E. (G) GABA immunohistochemistry results from a 35µm thick section of the *Xenopus laevis* brain. The cell body of the neuron from part C is circled in white. A 3X optical zoom was used. Scale bar represents 50µm.

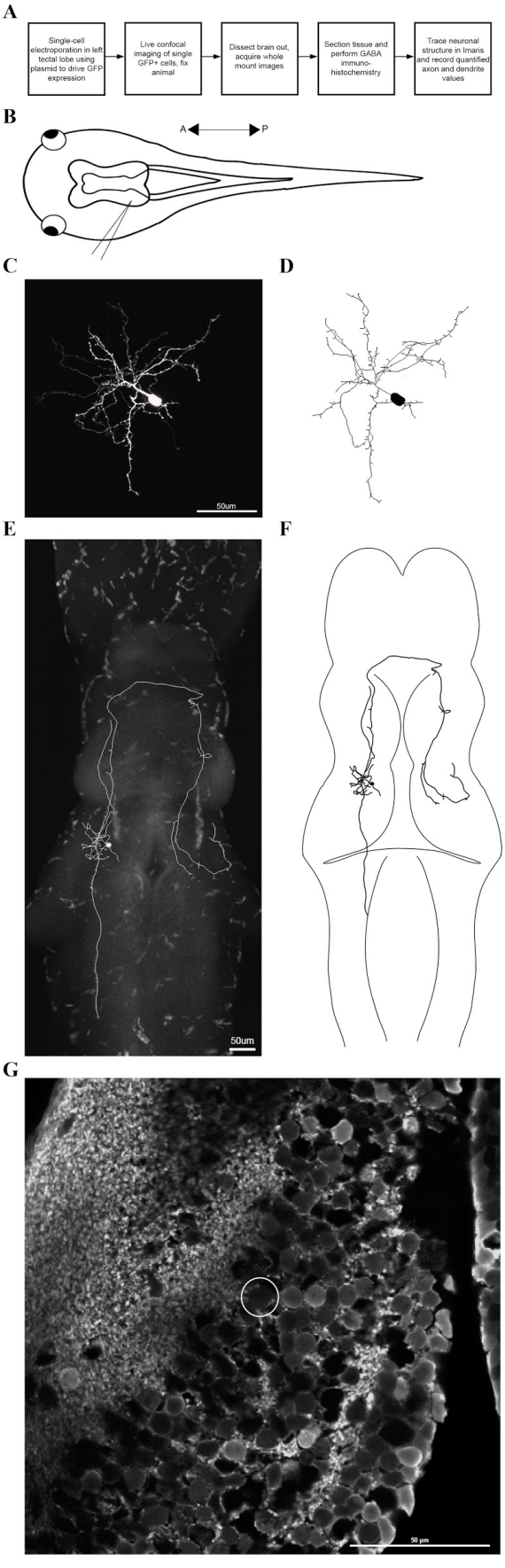
A
Single-cell electroporation in left tectal lobe using plasmid to drive GFP expression
Live confocal imaging of single GFP+ cells, fix animal
Dissect brain out, acquire whole mount images
Section tissue and perform GABA immuno-histochemistry
Trace neuronal structure in Imaris and record quantified axon and dendrite values
B
A
P
C
50um
D
E
50um
F
G
50 µm

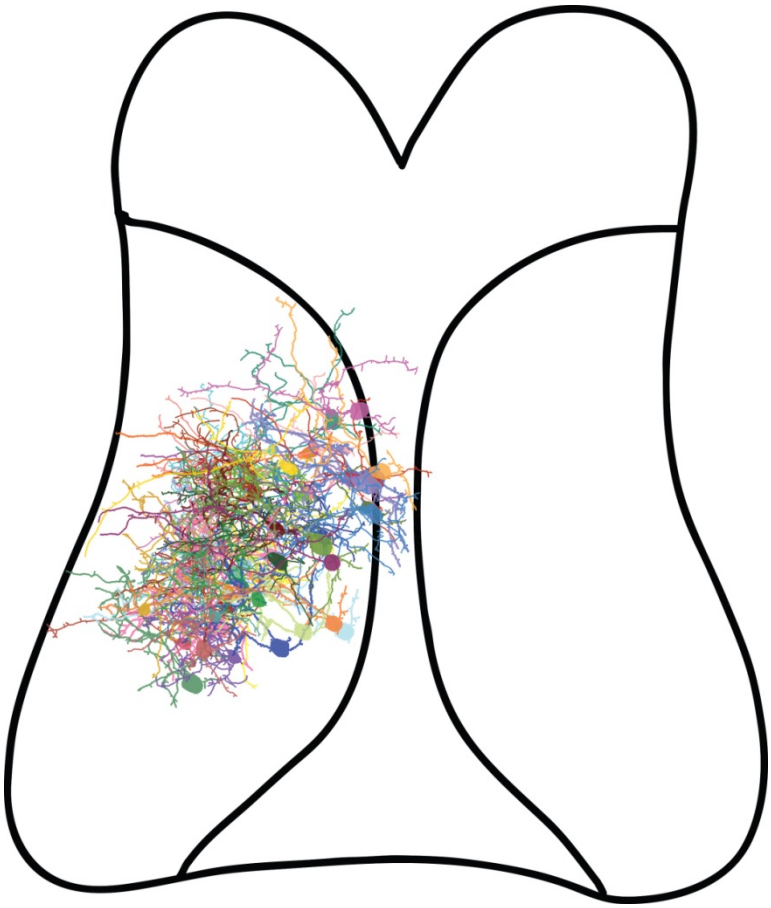

Figure 6. Schematic of the Xenopus laevis optic tectum with overlays of the dendritic reconstructions from all neurons analyzed. Location and orientation of the neurons are based on the whole-mount brain images of the neurons. Different colors represent different neurons.

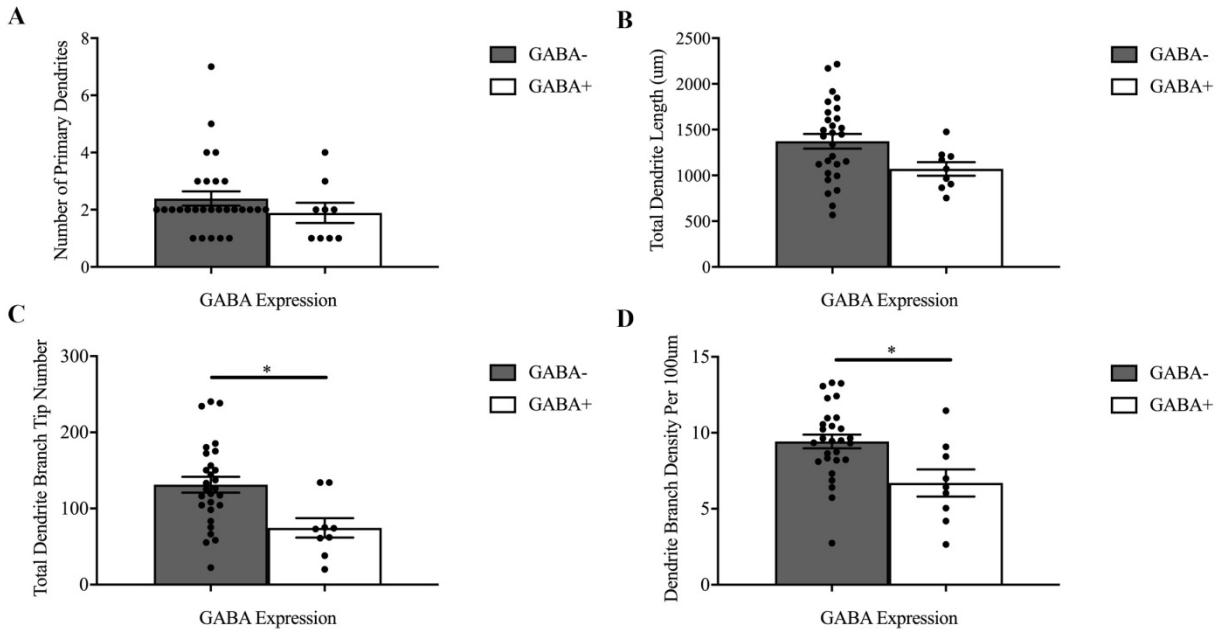

Figure 7. Results of dendritic morphology analyses of neurons in the Xenopus laevis optic tectum. Standard error of mean bars are shown. Data from individual neurons are also depicted as data points on all graphs. N=28 for GABA- (excitatory) neurons and N=9 for GABA+ (inhibitory) neurons. Grey bars represent data from excitatory neurons and white bars represent data from inhibitory neurons. Data were quantified in Imaris based on dendritic reconstructions of neurons. (A) Bar graph comparing the number of primary dendrites between excitatory and inhibitory neurons. Excitatory neurons had 2.39 ± 0.24 primary dendrites and inhibitory neurons had 1.89 ± 0.35 primary dendrites (p=0.2546, Mann-Whitney test). (B) Bar graph comparing the total dendrite length in micrometers between excitatory and inhibitory neurons. The total dendrite lengths were 1373 ± 80.80µm for excitatory neurons and 1071 ± 74.42µm for inhibitory neurons (p=0.051, Student's t-test). (C) Bar graph comparing the total dendrite branch tip number between excitatory and inhibitory neurons. Excitatory neurons had 131.1 ± 10.34 branch tips, while inhibitory neurons had 74.56 ± 12.76 branch tips. The horizontal bar and asterisk denotes a significant difference between the two bars, p=0.007 (Student's t-test). (D) Bar graph comparing the dendrite branch density per 100µm between excitatory and inhibitory neurons. This was calculated by the formula:
$Dendrite\ Branch\ Density\ = \frac{Total\ Dendrite\ Branch\ Tip\ Number}{Total\ Dendrite\ Length\ (\mu m)} \times 100$. Excitatory neurons had a dendrite branch density of 9.43 ± 0.45 branch tips/100µm while inhibitory neurons had a dendrite branch density of 6.703 ± 0.89 branch tips/100µm. The horizontal bar and asterisk denotes a significant difference between the two bars, p=0.007 (Student's t-test).

Figure 8. Depiction of workflow used to measure and analyze the deepest dendrite of neurons in the Xenopus laevis optic tectum. (A) Schematic of a lateral view of the optic tectum and hindbrain. A neuron is depicted in black, as well as retinal ganglion cell (RGC) axons in green and hindbrain axons in orange projecting to different depths of the tectum. (B) Dendritic reconstructions of two different neurons, produced based on the live images of the neurons. (C) The neurons in part B, rotated to an XZ plane, with depth measurements. The horizontal dashed lines represent where the measurement was taken as the deepest dendrite of each cell. (D) Bar graph comparing the deepest dendrite depth in micrometers between excitatory and inhibitory neurons. Data from individual neurons are also depicted as data points. N=28 for GABA- (excitatory) neurons and N=8 for GABA+ (inhibitory) neurons. Standard error of mean bars are shown. Grey bars represent data from excitatory neurons and white bars represent data from inhibitory neurons. The deepest dendrites of excitatory neurons were 99.04 ± 6.22μm in depth, and 108.2 ± 15.91μm for inhibitory neurons (p=0.522, Student's t-test).

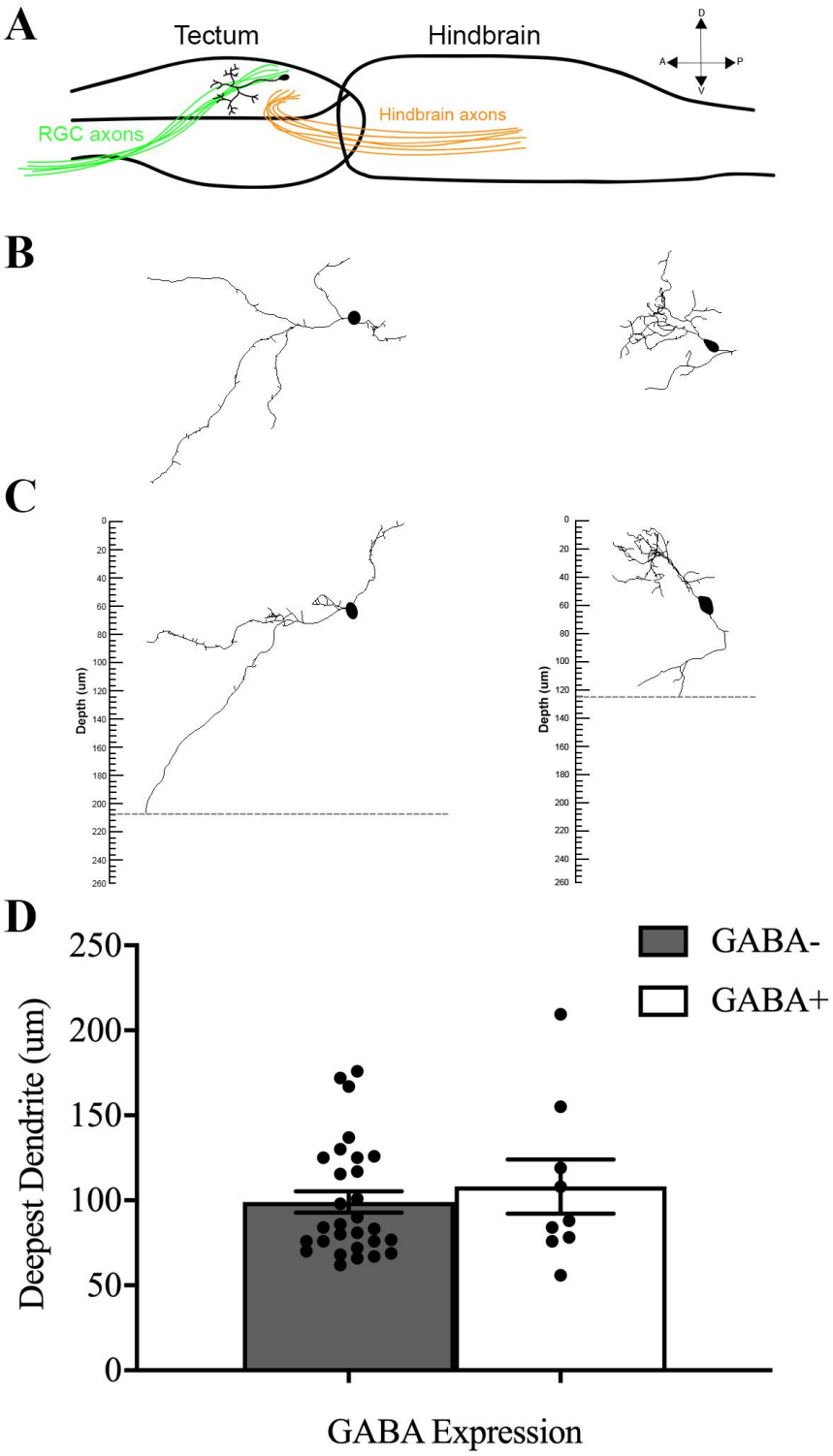
A
Tectum
Hindbrain
D
A
P
V
RGC axons
Hindbrain axons
B
C
Depth (um)
0
20
40
60
80
100
120
140
160
180
200
220
240
260
D
GABA-
GABA+
Deepest Dendrite (um)
250
200
150
100
50
0
GABA Expression

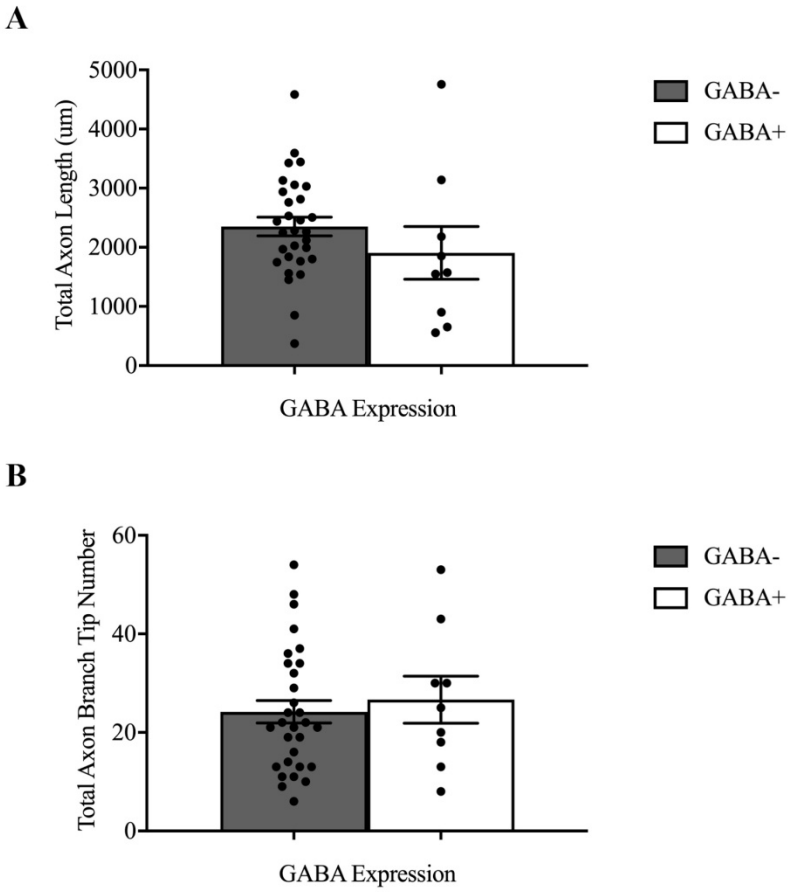

Figure 9. Results of axonal morphology analyses of neurons in the Xenopus laevis optic tectum. Standard error of mean bars are shown. Data from individual neurons are also depicted as data points on both graphs. N=30 for GABA- (excitatory) neurons and N=9 for GABA+ (inhibitory) neurons. Grey bars represent data from excitatory neurons and white bars represent data from inhibitory neurons. Data were quantified in Imaris based on axonal reconstructions of neurons. (A) Bar graph comparing the total axon length in micrometers between excitatory and inhibitory neurons. The average total axon length was 2352 ± 156.3µm for excitatory neurons and 1907 ± 446.5µm for inhibitory neurons (p=0.240, Student's t-test). (B) Bar graph comparing the total axon branch tip number between excitatory and inhibitory neurons. The average total of axon branch tips was 24.2 ± 2.29 branch tips for excitatory neurons and 26.67 ± 4.78 branch tips for inhibitory neurons (p=0.619, Student's t-test).

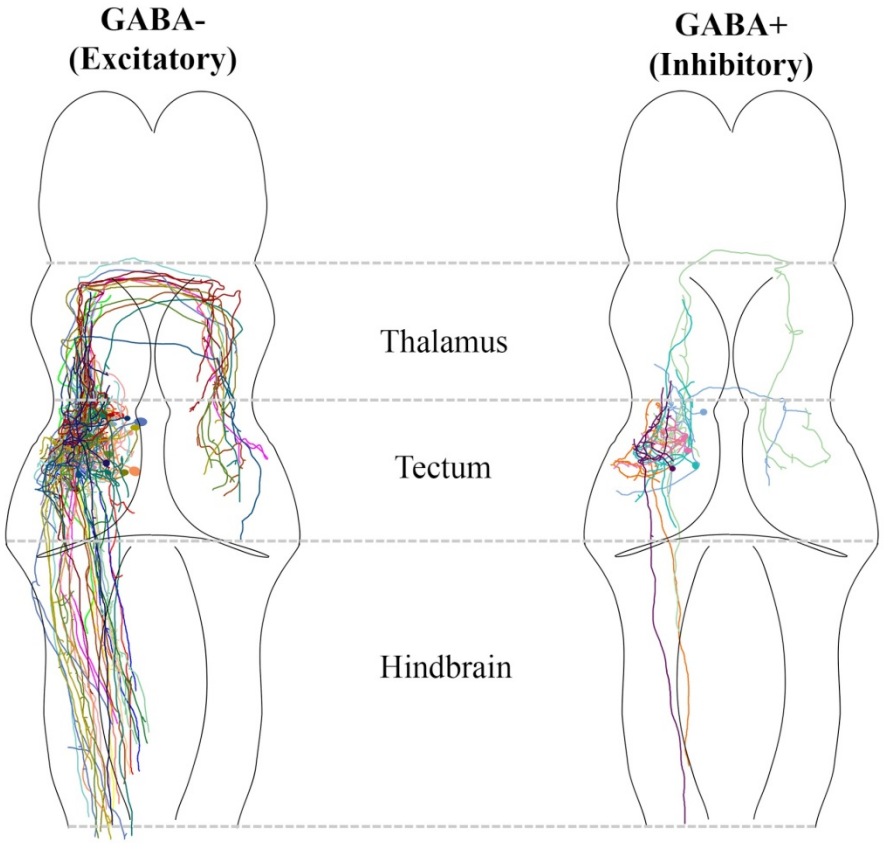

Figure 10. Schematic of a dorsal view of the Xenopus laevis whole brain with overlays of the axonal reconstructions from all neurons analyzed. Location and orientation of the neurons are based on the whole-mount brain images of the neurons. Different colors represent different neurons. The different regions labeled are the target locations analyzed as axon projection sites for Figure 11. The tegmentum is not shown as it is located ventrally underneath the tectum, and is not visible from a dorsal view.

Figure 11. Results of analyses of axon projection sites for neurons in the Xenopus laevis optic tectum. Standard error of mean bars and data points of individual neurons are shown for parts B and C. N=30 for GABA- (excitatory) neurons and N=9 for GABA+ (inhibitory) neurons. Grey bars represent data from excitatory neurons and white bars represent data from inhibitory neurons. Data were quantified based on axonal reconstructions of neurons. Axon target locations are depicted in Figure 10. The locations are ipsilateral and contralateral in reference to the soma located in the left tectal lobe. Horizontal bar with asterisk denotes significance between two bars. (A) Bar graph comparing the proportion of excitatory and inhibitory neurons that project to each of the target locations. 83.3% of excitatory neurons and 44.4% of inhibitory neurons analyzed had axons projecting ipsilaterally to the hindbrain (p=0.019, Chi-square test). All other proportions of cells projecting to the other target locations are not significantly different between excitatory and inhibitory neurons (p>0.05, Chi-square test). (B) Bar graph comparing the proportion of axon branch tips of each cell that are located in each target region, including cells that have 0 axon branch tips in each location. The proportions were calculated using the formula: $Proportion\ of\ Axon\ Branch\ Tips\ per\ Target\ = \frac{Number\ of\ Axon\ Branch\ Tips\ of\ Cell\ in\ Target}{Total\ Number\ of\ Axon\ Branch\ Tips\ of\ Cell}$. Excitatory neurons had a proportion of 0.1554 ± 0.028 of their axon branch tips located in the hindbrain. Inhibitory neurons had a proportion of 0.023 ± 0.01 of their axon branch tips located in the hindbrain (p=0.002, Mann-Whitney test). All other proportions of axon branch tips in all other target locations were not significantly different between excitatory and inhibitory neurons (p>0.05, Mann-Whitney test). (C) Bar graph comparing the average number of axon branch tips in each target location, excluding data from neurons without branch tips in each location. Average values were calculated using the formula: $Average\ Axon\ Branch\ Tip\ Number\ = \frac{Total\ Number\ of\ Axon\ Branch\ Tips\ in\ Target}{Number\ of\ Cells\ with\ Axon\ Projections\ in\ Target}$ for each target location. In the contralateral tectum, excitatory neurons had 2.17 ± 0.48 branch tips, while inhibitory neurons had 6.33 ± 1.86 branch tips (p=0.048, Mann-Whitney test). All other average amounts of axon branch tips in all other target locations were not significantly different between excitatory and inhibitory neurons (p>0.05, Mann-Whitney test).

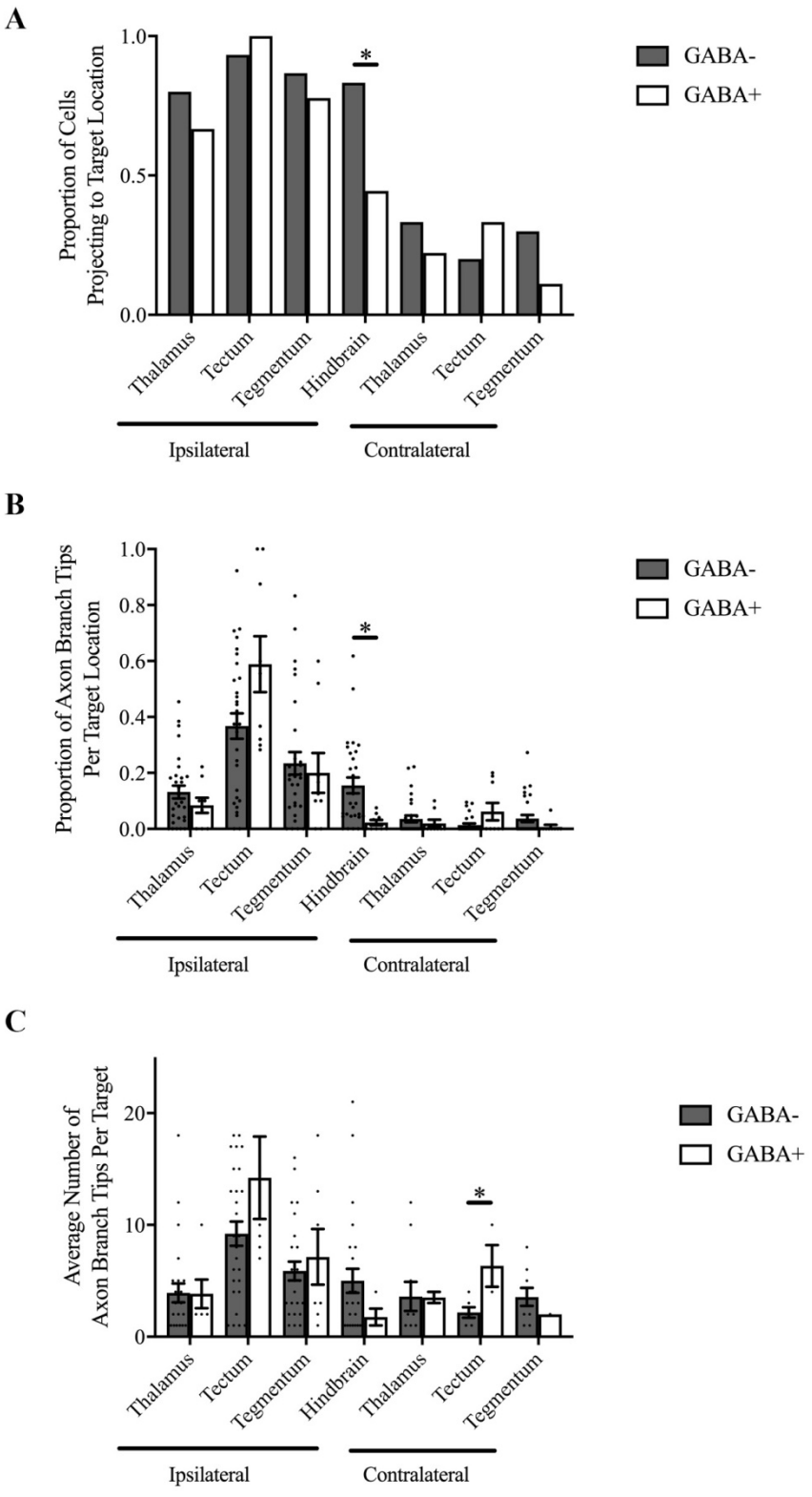
A
Proportion of Cells Projecting to Target Location
1.0
0.5
0.0
*
GABA-
GABA+
Thalamus
Tectum
Tegmentum
Hindbrain
Thalamus
Tectum
Tegmentum
Ipsilateral
Contralateral
B
Proportion of Axon Branch Tips Per Target Location
1.0
0.8
0.6
0.4
0.2
0.0
*
GABA-
GABA+
Thalamus
Tectum
Tegmentum
Hindbrain
Thalamus
Tectum
Tegmentum
Ipsilateral
Contralateral
C
Average Number of Axon Branch Tips Per Target
20
10
0
*
GABA-
GABA+
Thalamus
Tectum
Tegmentum
Hindbrain
Thalamus
Tectum
Tegmentum
Ipsilateral
Contralateral

Table 1. Trials used for experimenting with the SWITCH protocol for GABA immunohistochemistry in the Xenopus laevis optic tectum. Paraformaldehyde is abbreviated as PFA. Glutaraldehyde is abbreviated as GA. Hours and days are abbreviated as h and d, respectively. Room temperature is abbreviated as RT.

	Trial #1	Trial #2	Trial #3	Trial #4	Trial #5	Trial #6
Fixative	4% PFA + 2% GA, 1d 4C	4% PFA + 2% GA, 1d 4C	4% PFA + 2% GA, 1d 4C	4% PFA + 2% GA, 1d 4C	4% PFA + 2% GA, 1d 4C	4% PFA + 2% GA, 1d 4C
Fixation OFF	2d at 4C	1d at 4C	1d at 4C	2d at 4C	---	---
Fixation ON	1d at 4C	1d at 4C	1d at 4C	1d at 4C	---	---
PBST	Wash 2x, 4h each RT	Wash 2x, 4h each RT	Wash 2x, 4h each RT	Wash 2x, 4h each RT	---	---
Fixative Inactivation	1d at 37C	1d at 37C	1d at 37C	1d at 37C	1d at 37C	1d at 37C
Thermal Clearing	4d at 37C	4d at 37C	7d at 37C	7d at 37C	4d at 37C	7d at 37C
Antibody OFF	2d at 37C	2d at 37C	2d at 37C	2d at 37C	2d at 37C	2d at 37C
Antibody ON	1d at 37C	1d at 37C	1d at 37C	1d at 37C	1d at 37C	1d at 37C
Secondary Antibody	2h at RT	2h at RT	2h at RT	2h at RT	2h at RT	2h at RT
Nuclear Stain	DAPI 10min at RT	DAPI 10min at RT	DAPI 10min at RT	DAPI 10min at RT	DAPI 10min at RT	DAPI 10min at RT
Optical Clearing	FocusClear	FocusClear	FocusClear	FocusClear	FocusClear	FocusClear

	Trial #7	Trial #8	Trial #9	Trial #10	Trial #11	Trial #12
Fixative	4% PFA + 2% GA, 1d 4C	4% PFA + 4% GA, 1d 4C	4% PFA + 2% GA, 1d 4C	4% PFA + 4% GA, 1d 4C	4% PFA +2% GA, 1d 4C	4% PFA +2% GA, 1d 4C
Quenching	1% NaBH, 10 min RT	1% NaBH, 10 min RT	1% NaBH, 10 min RT	1% NaBH, 10 min RT	1% NaBH, 10 min RT	1% NaBH, 10 min RT
PBST	1% PBST, 1h RT	1% PBST, 1h RT	1% PBST, 1h RT	1% PBST, 1h RT	2% PBST, 1 h RT	2% PBST, 1h RT
Thermal Clearing	2d at 37C	2d at 37C	1d at 37C	1d at 37C	6h at 37C	---
Antibody OFF	6h at 37C	6h at 37C	1d at 37C	1d at 37C	2d at 37C	2d at 37C
Antibody ON	1d at 37C	1d at 37C	1d at 37C	1d at 37C	1d at 37C	1d at 37C
Secondary Antibody	2h at RT	2h at RT	2h at RT	2h at RT	2h at RT	2h at RT
Nuclear Stain	DAPI 10min at RT	DAPI 10min at RT	DAPI 10min at RT	DAPI 10min at RT	DAPI 10min at RT	DAPI 10min at RT
Optical Clearing	FocusClear	FocusClear	FocusClear	FocusClear	FocusClear	FocusClear

	Trial #13	Trial #14	Trial #15	Trial #16	Trial #17	Trial #18
Fixative	4% PFA + 2% GA, 1d 4C	4% PFA + 2% GA, 1d 4C	4% PFA + 2% GA, 1d 4C	4% PFA + 2% GA, 1d 4C	4% PFA + 2% GA, 1d 4C	4% PFA + 2% GA, 1d 4C
Quenching	1% NaBH, 10 min RT	1% NaBH, 10 min RT	1% NaBH, 10 min RT	1% NaBH, 10 min RT	1% NaBH, 10 min RT	1% NaBH, 10 min RT
PBST	2% PBST, 1hr, RT	2% PBST, 1hr, RT	2% PBST, 1hr, RT	2% PBST, 1hr, RT	2% PBST, 1hr, RT	2% PBST, 1hr, RT
Thermal Clearing	1d at 37C	1d at RT	1d at 4C	2d at 4C	1d at 37C	2d at 37C
Antibody OFF	3d at 37C	3d at RT	3d at 4C	3d at 4C	3d at 4C	3d at 4C
Antibody ON	1d at 37C	1d at RT	1d at 4C	1d at 4C	1d at 4C	1d at 4C
Secondary Antibody	2hr at RT	2hr at RT	2hr at RT	2hr at RT	2hr at RT	2hr at RT
Nuclear Stain	DAPI 10 min RT	DAPI 10 min RT	DAPI 10 min RT	DAPI 10 min RT	DAPI 10 min RT	DAPI 10 min RT
Optical Clearing	FocusClear	FocusClear	FocusClear	FocusClear	FocusClear	FocusClear

	Trial #19	Trial #20	Trial #21
Fixative	4% PFA + 2% GA, 1d 4C	4% PFA + 2% GA, 1d 4C	4% PFA + 2% GA, 1d 4C
Quenching	1% NaBH, 10 min RT	1% NaBH, 10 min RT	1% NaBH, 10 min RT
PBST	2% PBST, 1hr, RT	2% PBST, 1hr, RT	2% PBST, 1hr, RT
Thermal Clearing	2d at 4C	2d at 4C	1d at 37C
Antibody OFF	3d at 4C	7d at 4C	---
Antibody ON	1d at 4C	1d at 4C	Regular Primary (3d at 4C)
Secondary Antibody	2hr at RT	2hr at RT	2hr at RT
Nuclear Stain	DAPI 10 min RT	DAPI 10 min RT	DAPI 10 min RT
Optical Clearing	FocusClear	FocusClear	FocusClear

Table 2. Trials used for experimenting with the SWITCH protocol for PH3 and β-tubulin immunohistochemistry in the Xenopus laevis optic tectum. Paraformaldehyde is abbreviated as PFA. Glutaraldehyde is abbreviated as GA. Hours and days are abbreviated as h and d, respectively. Room temperature is abbreviated as RT.

	Trial #1		Trial #2		Trial #3		Trial #4	
Antibody	PH3	B-tubulin	PH3	B-tubulin	PH3	B-tubulin	PH3	B-tubulin
Fixative	4% PFA, 1d 4C	4% PFA, 1d 4C	4% PFA, 1d 4C	4% PFA, 1d 4C	4% PFA + 2% GA, 1d 4C	4% PFA + 2% GA, 1d 4C	4% PFA, 1d 4C	4% PFA, 1d 4C
Quenching	1% NaBH, 10 min RT	1% NaBH, 10 min RT	1% NaBH, 10 min RT	1% NaBH, 10 min RT	1% NaBH, 10 min RT	1% NaBH, 10 min RT	1% NaBH, 10 min RT	1% NaBH, 10 min RT
PBST	2% PBST, 1hr, RT	2% PBST, 1h RT	2% PBST, 1hr, RT	2% PBST, 1hr, RT	2% PBST, 1h RT	2% PBST, 1h RT	2% PBST, 1h RT	2% PBST, 1h RT
Thermal Clearing	2d at 4C	2d at 4C	2d at 37C	2d at 37C	2d at 37C	2d at 37C	2d at 4C	2d at 4C
Antibody OFF	5d at 4C	5d at 4C	4d at 37C	4d at 37C	2d at 37C	2d at 37C	---	---
Antibody ON	1d at 4C	1d at 4C	1d at 37C	1d at 37C	3d at 37C	3d at 37C	Regular Primary (1d at 4C)	Regular Primary (1d at 4C)
Secondary Antibody	2hr at RT	2hr at RT	2hr at RT	2hr at RT	2hr at RT	2 hr at RT	2hr at RT	2 hr at RT
Nuclear Stain	Sytox-O, 10 min RT	Sytox-O, 10 min RT	DAPI 10 min RT	DAPI 10 min RT	Sytox-O, 10 min RT	Sytox-O, 10 min RT	Sytox-O, 10 min RT	Sytox-O, 10 min RT
Optical Clearing	FocusClear	FocusClear	FocusClear	FocusClear	FocusClear	FocusClear	FocusClear	FocusClear

REFERENCES

(PING), T. P. I. N. G., Ascoli, G. A., Alonso-Nanclares, L., Anderson, S. A., Barrionuevo, G., Benavides-Piccione, R., Burkhalter, A., Buzsáki, G., Cauli, B., DeFelipe, J., Fairén, A., Feldmeyer, D., Fishell, G., Fregnac, Y., Freund. T. F., Gardner, D., Gardner, E. P., Goldberg, J. H., Helmstaedter, M., Hestrin, S., Karube, F., Kisvárday, Z. F., Lambolez, B., Lewis, D. A., Marin, O., Markram, H., Muñoz, A., Packer, A., Petersen, C. C. H., Rockland, K. S., Rossier, J., Rudy, B., Somogyi, P., Staiger, J. F., Tamas, G., Thomson, A. M., Toledo-Rodriguez, M., Wang, Y., West, D. C., & Yuste, R. (2008). Petilla terminology: nomenclature of features of GABAergic interneurons of the cerebral cortex. *Nature Reviews Neuroscience*, *9*(7), 557–568. https://doi.org/10.1038/nrn2402

Aizenman, C. D., & Cline, H. T. (2007). Enhanced Visual Activity In Vivo Forms Nascent Synapses in the Developing Retinotectal Projection. *Journal of Neurophysiology*, *97*(4), 2949–2957. https://doi.org/10.1152/jn.00452.2006

Akerman, C. J. (2006). Depolarizing GABAergic Conductances Regulate the Balance of Excitation to Inhibition in the Developing Retinotectal Circuit In Vivo. *Journal of Neuroscience*, *26*(19), 5117–5130. https://doi.org/10.1523/JNEUROSCI.0319-06.2006

Akerman, C. J., & Cline, H. T. (2007). Refining the roles of GABAergic signaling during neural circuit formation. *Trends in Neurosciences*, *30*(8), 382–389. https://doi.org/10.1016/J.TINS.2007.06.002

Benavides-Piccione, R., Hamzei-Sichani, F., Ballesteros-Yáñez, I., Defelipe, J., & Yuste, R. (2006). Dendritic size of pyramidal neurons differs among mouse cortical regions. *Cerebral Cortex*, *16*(7), 990–1001. https://doi.org/10.1093/cercor/bhj041

Bestman, J. E., Ewald, R. C., Chiu, S.-L., & Cline, H. T. (2006). In vivo single-cell electroporation for transfer of DNA and macromolecules. *Nature Protocols*, *1*(3), 1267–1272. https://doi.org/10.1038/nprot.2006.186

Bianco, I. H., & Engert, F. (2015). Visuomotor transformations underlying hunting behavior in zebrafish. *Current Biology : CB*, *25*(7), 831–846. https://doi.org/10.1016/j.cub.2015.01.042

Chiang, A. S., Lin, C. Y., Chuang, C. C., Chang, H. M., Hsieh, C. H., Yeh, C. W., Shih, C. T., Wu, J. J., Wang, G. T., Chen, Y. C., Wu, C. C., Chen, G. Y., Ching, Y. T., Lee, P. C., Lin, C. Y., Lin., H. H., Wu, C. C., Hsu, H. W., Huang, Y. A., Chen, J. Y., Chiang, H. J., Lu, C. F., Ni, R. F., Yeh, C. Y., Hwang, J. K. (2011). Three-dimensional reconstruction of brain-wide wiring networks in drosophila at single-cell resolution. *Current Biology*, *21*(1), 1–11. https://doi.org/10.1016/j.cub.2010.11.056

Chung, K., Wallace, J., Kim, S. Y., Kalyanasundaram, S., Andalman, A. S., Davidson, T. J., Mirzabekov, J. J., Zalocusky, K. A., Mattis, J., Denisin, A. K., Pak, S., Bernstein, H., Ramakrishnan, C., Grosenick, L., Gradinaru, V., & Deisseroth, K. (2013). Structural and molecular interrogation of intact biological systems. *Nature*, *497*(7449), 332–337. https://doi.org/10.1038/nature12107

Cline, H. T. (2001). Dendritic arbor development and synaptogenesis. *Current Opinion in Neurobiology*. Elsevier Current Trends. https://doi.org/10.1016/S0959-4388(00)00182-3

Felch, D. L., Khakhalin, A. S., & Aizenman, C. D. (2016). Multisensory integration in the developing tectum is constrained by the balance of excitation and inhibition. *ELife*, *5*(2016). https://doi.org/10.7554/elife.15600

Felsen, G., & Mainen, Z. F. (2012). Midbrain contributions to sensorimotor decision making. *Journal of Neurophysiology*, *108*(1), 135–147. https://doi.org/10.1152/jn.01181.2011

Fishell, G., & Heintz, N. (2013). The Neuron Identity Problem: Form Meets Function. *Neuron*, *80*(3), 602–612. https://doi.org/10.1016/J.NEURON.2013.10.035

Freifeld, L., Odstrcil, I., Förster, D., Ramirez, A., Gagnon, J. A., Randlett, O., Costa, E. K., Asano, S., Celiker, O. T., Gao, R., Martin-Alarcon, D. A., Reginato, P., Dick, C., Chen, L., Schoppik, D., Engert, F., Baier, H., & Boyden, E. S. (2017). Expansion microscopy of zebrafish for neuroscience and developmental biology studies. *Proceedings of the National Academy of Sciences*, *114*(50), E10799–E10808. https://doi.org/10.1073/pnas.1706281114

Gambrill, A. C., Faulkner, R. L., & Cline, H. T. (2016). Experience-dependent plasticity of excitatory and inhibitory intertectal inputs in *Xenopus* tadpoles. *Journal of Neurophysiology*, *116*(5), 2281–2297. https://doi.org/10.1152/jn.00611.2016

He, H.-Y., Shen, W., Hiramoto, M., & Cline, H. T. (2016). Experience-Dependent Bimodal Plasticity of Inhibitory Neurons in Early Development. *Neuron*, *90*(6), 1203–1214. https://doi.org/10.1016/J.NEURON.2016.04.044

Hiramoto, M., & Cline, H. T. (2009). Convergence of multisensory inputs in Xenopus tadpole tectum. *Developmental Neurobiology*, *69*(14), 959–971. https://doi.org/10.1002/dneu.20754

Kanari, L., Ramaswamy, S., Shi, Y., Morand, S., Meystre, J., Perin, R., Abdellah, M., Wang, Y., Hess, K., & Markram, H. (2019). Objective Morphological Classification of Neocortical Pyramidal Cells. *Cerebral Cortex (New York, N.Y. : 1991)*, *29*(4), 1719–1735. https://doi.org/10.1093/cercor/bhy339

King, A. J. (2004). The superior colliculus. *Current Biology : CB*, *14*(9), R335-8. https://doi.org/10.1016/j.cub.2004.04.018

Lázár, G. (1973). The development of the optic tectum in Xenopus laevis: a Golgi study. *Journal of Anatomy*, *116*(Pt 3), 347–355. Retrieved from http://www.ncbi.nlm.nih.gov/pubmed/4791391

Li, J., Erisir, A., & Cline, H. (2011). In Vivo Time-Lapse Imaging and Serial Section Electron Microscopy Reveal Developmental Synaptic Rearrangements. *Neuron*, *69*(2), 273–286. https://doi.org/10.1016/J.NEURON.2010.12.022

Li, Z., & Fite, K. V. (1998). Distribution of GABA-like immunoreactive neurons and fibers in the central visual nuclei and retina of frog, Rana pipiens. *Visual Neuroscience*, *15*(6), 995–1006. https://doi.org/10.1017/S0952523898155207

Liu, H.-H., & Cline, H. T. (2016). Fragile X Mental Retardation Protein Is Required to Maintain Visual Conditioning-Induced Behavioral Plasticity by Limiting Local Protein Synthesis. *The Journal of Neuroscience : The Official Journal of the Society for Neuroscience*, *36*(27), 7325–7339. https://doi.org/10.1523/JNEUROSCI.4282-15.2016

Liu, Z., Hamodi, A. S., & Pratt, K. G. (2016). Early development and function of the Xenopus tadpole retinotectal circuit. *Current Opinion in Neurobiology*, *41*, 17–23. https://doi.org/10.1016/J.CONB.2016.07.002

McKeown, C. R., Sharma, P., Sharipov, H. E., Shen, W., & Cline, H. T. (2013). Neurogenesis is required for behavioral recovery after injury in the visual system of *Xenopus laevis*. *Journal of Comparative Neurology*, *521*(10), 2262–2278. https://doi.org/10.1002/cne.23283

Miraucourt, L. S., da Silva, J. S., Burgos, K., Li, J., Abe, H., Ruthazer, E. S., & Cline, H. T. (2012). GABA expression and regulation by sensory experience in the developing visual system. *PLoS ONE*, *7*(1), e29086. https://doi.org/10.1371/journal.pone.0029086

Murray, E., Cho, J. H., Goodwin, D., Ku, T., Swaney, J., Kim, S.-Y., Choi, H., Park, Y.-G., Park, J.-Y., Hubbert, A., McCue, M., Vassallo, S., Bakh, N., Frosch, M. P., Wedeen, V. J., Seung,

H. S., & Chung, K. (2015). Simple, Scalable Proteomic Imaging for High-Dimensional Profiling of Intact Systems. *Cell*, *163*(6), 1500–1514. https://doi.org/10.1016/J.CELL.2015.11.025

Niell, C. M., Meyer, M. P., & Smith, S. J. (2004). In vivo imaging of synapse formation on a growing dendritic arbor. *Nature Neuroscience*, *7*(3), 254–260. https://doi.org/10.1038/nn1191

Nieuwkoop PD, Faber J. (1956) *Normal Table of Xenopus laevis (Daudin); a Systematical and Chronological Survey of the Development form the Fertilized Egg till the End of the Metamorphosis.* Amsterdam: North-Holland.

Ramón y Cajal S (1899) *La Textura del Sistema Nerviosa del Hombre y los Vertebrados*. Madrid: Moya (Primera Edicion).

Randlett, O., Wee, C. L., Naumann, E. A., Nnaemeka, O., Schoppik, D., Fitzgerald, J. E., Portugues, R., Lacoste, A. M. B., Riegler, C., Engert, F., & Schier, A. F. (2015). Whole-brain activity mapping onto a zebrafish brain atlas. *Nature Methods*, *12*(11), 1039–1046. https://doi.org/10.1038/nmeth.3581

Rybicka, K. K., & Udin, S. B. (1994). Ultrastructure and GABA Immunoreactivity in Layers 8 and 9 of the Optic Tectum of Xenopus laevis. *European Journal of Neuroscience*, *6*(10), 1567–1582. https://doi.org/10.1111/j.1460-9568.1994.tb00547.x

Tao, H. W., & Poo, M. (2005). Activity-dependent matching of excitatory and inhibitory inputs during refinement of visual receptive fields. *Neuron*, *45*(6), 829–836. https://doi.org/10.1016/j.neuron.2005.01.046

Tasic, B., Menon, V., Nguyen, T. N., Kim, T. K., Jarsky, T., Yao, Z., Levi, B., Gray, L. T., Sorensen, S. A., Dolbeare, T., Bertagnolli, D., Goldy, J., Shapovalova, N., Parry, S., Lee, C., Smith, K., Bernard, A., Madisen, L., Sunkin, S. M., Hawrylycz, M., Koch, C., & Zeng, H. (2016). Adult mouse cortical cell taxonomy revealed by single cell transcriptomics. *Nature Neuroscience*, *19*(2), 335–346. https://doi.org/10.1038/nn.4216

Tasic, B., Yao, Z., Graybuck, L. T., Smith, K. A., Nguyen, T. N., Bertagnolli, D., Goldy, J., Garren, E., Economo, M. N., Viswanathan, S., Penn, O., Bakken, T., Menon, V., Miller, J., Fong, O., Hirokawa, K. E., Lathia, K., Rimorin, C., Tieu, M., Larsen, R., Casper, T., Barkan, E., Kroll, M., Parry, S., Shapovalova, N. V., Hirschstein, D., Pendergraft, J., Sullivan, H. A., Kim, T. K., Szafer, A., Dee, N., Groblewski, P., Wickersham, I., Cetin, A.,

Harris, J. A., Levi, B. P., Sunkin, S. M., Madisen, L., Daigle, T. L., Looger, L., Bernard, A., Phillips, J., Lein, E., Hawrylycz, M., Svoboda, K., Jones, A. R., Koch, C., & Zeng, H. (2018). Shared and distinct transcriptomic cell types across neocortical areas. *Nature*, *563*(7729), 72–78. https://doi.org/10.1038/s41586-018-0654-5

Wang, X., Tucciarone, J., Jiang, S., Yin, F., Wang, B. S., Wang, D., Jia, Y., Jia, X., Li, Y., Yang, T., Xu, Z., Akram, M. A., Wang, Y., Zeng, S., Ascoli, G. A., Mitra, P., Gong, H., Luo, Q., & Huang, Z. J. (2019). Genetic Single Neuron Anatomy Reveals Fine Granularity of Cortical Axo-Axonic Cells. *Cell Reports*, *26*(11), 3145–3159.e5. https://doi.org/10.1016/j.celrep.2019.02.040

Wang, Y., Ye, M., Kuang, X., Li, Y., & Hu, S. (2018). A simplified morphological classification scheme for pyramidal cells in six layers of primary somatosensory cortex of juvenile rats. *IBRO Reports*, *5*(October), 74–90. https://doi.org/10.1016/j.ibror.2018.10.001